UNIVERSITÀ DEGLI STUDI DI PADOVA
DIPARTIMENTO DI INGEGNERIA INDUSTRIALE
CORSO DI LAUREA IN INGEGNERIA CHIMICA E DEI PROCESSI INDUSTRIALI

Tesi di Laurea Magistrale in
Ingegneria Chimica e dei Processi Industriali

THERMAL DECOMPOSITION OF TRICYCLOHEXYLIDENE TRIPEROXIDE USING FLOW CHEMISTRY TECHNIQUES

Relatore: Prof. Giuseppe Maschio
Correlatore: Prof. Julià Sempere

Laureando: Valentino Fort

ANNO ACCADEMICO 2017 – 2018

Abstract

Flow chemistry has been applied in many classic organic syntheses over the past several years and has given the chance to replace the traditional batch processes commonly used in fine chemicals industry. Continuous processes are safer and more efficient.

In this work, flow chemistry techniques are applied to the production of 16-hexadecanolide, a high value macrolactone used in cosmetic industry as an ingredient of musk aroma. It is obtained from the thermal decomposition of tricyclohexylidene triperoxide, a synthetic route proposed by Story in 1968. The reaction is extremely exothermic, so it can't be performed in batch.

A preliminary set of batch experiments is designed to understand the conditions to be further applied in the continuous system. Reagent's concentration, temperature and reaction time are investigated.

Two flow configurations are built and operated: the tubular reactor and the tube-in-tube reactor. With the second layout, a gas permeable membrane made of Teflon® AF-2400 is used to extract the CO_2 that is generated while tricyclohexylidene triperoxide is reacting. The reaction is carried out at 170°C, so the extraction of CO_2 protects the system from collapsing in the eventuality of sudden gas expansion.

The conversion profile of the tube-in-tube reactor is predicted with good accuracy using a laminar flow reactor (LFR) model, developed and implemented in MATLAB®. It is demonstrated that CO_2 generation affects the fluid dynamics of the system.

The concentration of 16-hexadecanolide in the crude reaction mixture is evaluated using High performances liquid chromatography (HPLC). A final yield of 17 % is calculated.

Riassunto

Si applicano le tecniche di flow chemistry alla reazione di decomposizione termica del triperossido di tricicloesilidene. La reazione, formalizzata per la prima volta da Story nel 1968, permette di ottenere 16-esadecanolide, un macrolattone ciclico usato nell'industria cosmetica come ingrediente della fragranza al muschio bianco, in sostituzione della materia prima naturale.

La reazione è fortemente esotermica e libera CO_2 al procedere della conversione. Non può essere condotta in sicurezza in un reattore discontinuo.

In questa tesi si vuole provare l'efficacia dell'impiego di reattori continui nella conduzione in sicurezza della decomposizione termica del triperossido di tricicloesilidene.

Si è sviluppato un primo disegno sperimentale con sistema discontinuo per l'identificazione delle condizioni di reazione più idonee all'interno del dominio sperimentale selezionato. Si è indagato l'effetto dei fattori temperatura, quantità di reagente iniziale e tempo di reazione sulle variabili conversione, selettività e resa nel prodotto desiderato (16-esadecanolide). Si è concluso che le condizioni alle quali operare il processo continuo sono: temperatura di reazione di 170°C, frazione di reagente iniziale uguale a 4 % p/p e tempo di reazione sufficiente a raggiungere completa conversione del triperossido.

Si è progettato e realizzato un reattore tubulare continuo del diametro interno di 0.03". Si sono ricavati i profili di conversione, di selettività e di resa in funzione del tempo di residenza.

Si è progettato e realizzato un reattore continuo *tube-in-tube* del diametro interno di 0.032". Si tratta di un reattore a due tubi concentrici. Il materiale con cui è realizzato il tubo interno è un polimero fluorurato amorfo (Teflon® AF-2400) permeabile ai gas. Applicando il vuoto nello spazio anulare compreso tra i due tubi, è possibile estrarre la CO_2 generata dalla decomposizione.

La resa complessiva dei due processi continui è confrontabile e uguale a 0.17, a fronte di un massimo teorico di 1.

Si è sviluppato un modello di reattore in flusso laminare (LFR) per la previsione del profilo di conversione al variare del tempo di residenza. Si è dimostrato che la generazione di CO_2 influisce sulla fluidodinamica del sistema. I dati sperimentali ottenuti con il reattore *tube-in-tube* sono correttamente prevedibili utilizzando il modello LFR.

Si conclude che il reattore *tube-in-tube* fornisce uno strumento più sicuro e affidabile per condurre in continuo la decomposizione termica del triperossido di tricicloesilidene.

Index

Introduction

The Synthesis of Story provides a straightforward way to obtain 16-hexadecanolide, a cyclic macrolactone. It is a high-value molecule used in cosmetic industry as the main component of musk aroma. It was historically extracted from animals, an expensive and not sustainable way to obtain the fragrance (Story *et al.*, 1968)

The synthetic route to 16-hexadecanolide proposed by Story is attractive from an industrial point of view because it requires common reagents like cyclohexanone and hydrogen peroxide to obtain tricyclohexylidene triperoxide, a stable intermediate which is subsequently thermally decomposed to produce 16-hexadecanolide(Williams, 1999).

This work is focused on the thermal decomposition of tricyclohexylidene triperoxide, a strongly exothermic reaction accompanied by CO_2 generation. Those features make the process a good candidate to apply flow chemistry techniques, since a batch reactor is not a safe possibility.

Flow chemistry basically consist of a process in which reagents and products are respectively fed and extracted continuously. During the last twenty years, flow chemistry adopted the concepts of process intensification and applied them to reactors design.

The tube-in-tube reactor, for example, was recently used to perform many organic syntheses in which gas phase reactants are involved. It is a two concentric tubes reactor, whose inner tube is made of Teflon® AF-2400, a gas permeable membrane (Brzozowski *et al.*, 2015). In this thesis, this reactor layout will be used, but for the reverse operation: the gaseous by-product extraction.

In particular, the aim of this work is to design a reactor to safely perform the decomposition of tricyclohexylidene triperoxide in a continuous basis. Reducing the volumes of reacting mixture with respect to batch operation, removing the gas produced and correctly predicting the residence time are some of the issues that will be solved in the following chapters.

In view of the above, this work is going to be developed in three steps:

1) A set of batch experiments to explore the general features of the reaction, to confirm the previous works results and to identify the best operating conditions.
2) Performing the reaction in continuous using a tubular reactor and understanding the effect of CO_2 formation on conversion profile.
3) Building the tube-in-tube reactor, using it to perform the thermolysis of tricyclohexylidene triperoxide and compare its performance to the tubular reactor's ones.

The development of those objectives is organised in five chapters.

Chapter 1 provides a brief introduction to the synthesis of Story and to its application in the production of macrocyclic lactones and hydrocarbons. An overview on flow chemistry

techniques in their specific application to tricyclohexylidene triperoxide decomposition follows.

In Chapter 2 general concepts of thermal analysis and autocatalytic reactions are summarised. It is then reported the explanation of the kinetic model of tricyclohexylidene triperoxide thermal decomposition.

Chapter 3 is about synthesis and batch decomposition of tricyclohexylidene triperoxide. A design of experiments is carried out to understand the best conditions to perform the reaction inside the experimental domain.

Chapter 4 is devoted to flow reactors. The experimental conversion at different residence time are reported using a tubular reactor and a tube-in-tube reactor. Both PFR and LFR models are used to predict the conversion profiles of the reactors.

In Chapter 5 the experimental procedures to obtain data are reported: materials, equipment, analytical techniques and reactors build-up.

Chapter 1

Flow chemistry and fine chemicals

In this chapter a brief introduction to the Synthesis of Story is carried out. It is explained how to obtain high added-value compound like macrocyclic lactones and hydrocarbons starting from hydrogen peroxide and cyclohexanone.
It follows an overview on flow chemistry techniques and about their application to tricyclohexylidene triperoxide decomposition.

1.1 The Synthesis of Story and macrolactones

Story *et al.* (1968) discovered the possibility to obtain macrocyclic compounds from the decomposition of ketone peroxides. High value macrocyclic hydrocarbons and macrocyclic lactones can be produced from tricyclohexylidene triperoxide (TCHP, Figure 1, left) and dicyclohexylidene diperoxide (DCHP, Figure 1, right), two cyclohexanone peroxides.

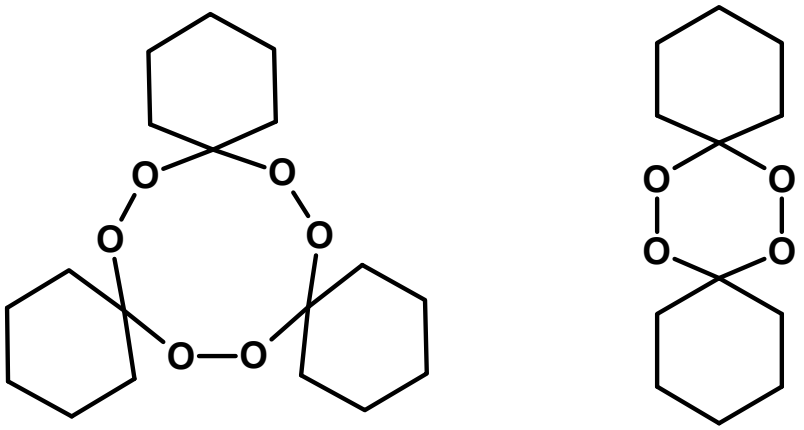

Figure 1. *Tricyclohexylidene triperoxide (left) and dicyclohexylidene diperoxide (right).*

The decomposition of the former yields 16-hexadecanolide (Figure 2), a macrocyclic lactone able to substitute the scarce raw material in the production of musk aroma from musk deer's scent glands.

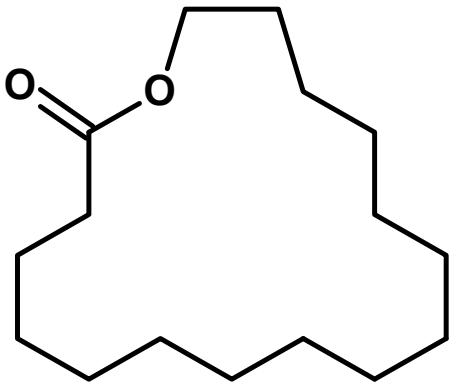

Figure 2. *16-hexadecanolide, a high value macrocyclic lactone used in cosmetic industry.*

They found out that the decomposition of the appropriate ketone peroxide provides a general and facile synthesis of a large variety of macrocyclic compounds (Bush and Story, 1970), suitable for high value applications, such as monomers for high flexibility and high hydrolysis resistant polyesters.
Moreover, they can be used to synthetize polyurethanes, thermoplastic polymers, adhesives, synthetic leather and fabrics, resins for surface coatings, microcells foams and orthopaedic supports.
The Synthesis of Story is basically made of two steps. The first one (§1.1.1) includes the synthesis of the cyclohexanone peroxides; the second one (§1.1.2) is about their decomposition.

1.1.1 Synthesis of cyclohexanone peroxides

The first procedure reported in literature (Story *et al.*, 1970) provides 70 % concentrated perchloric acid in acetonitrile as catalyst and 90 % concentrated hydrogen peroxide, in 2:1 molar ratio to cyclohexanone, at 70°C.
The main products are DCHP and TCHP. TCHP is the kinetically favoured product, whereas the diperoxide is the thermodynamically stable one.
Stoichiometric equations leading their formation are reported in Figure 3 and Figure 4.

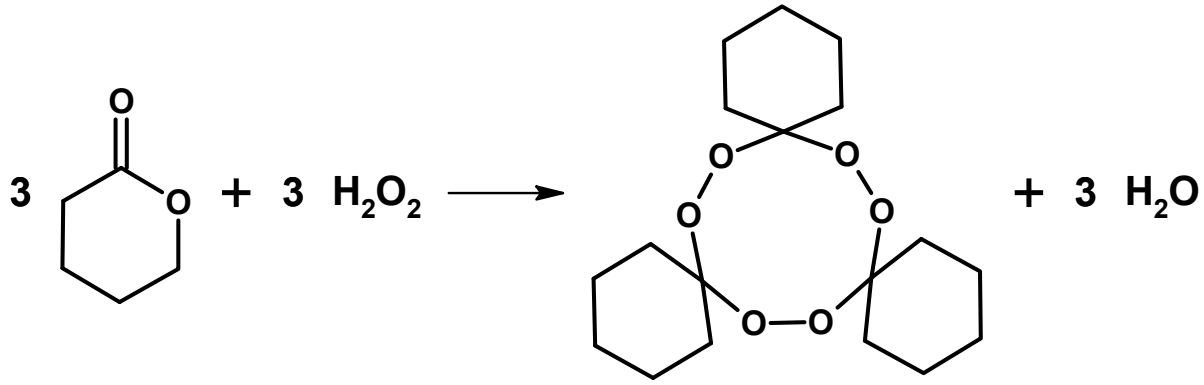

Figure 3. *First step of the Synthesis of Story: synthesis of tricyclohexylidene triperoxide via cyclohexanone oxidation using hydrogen peroxide and acid catalyst.*

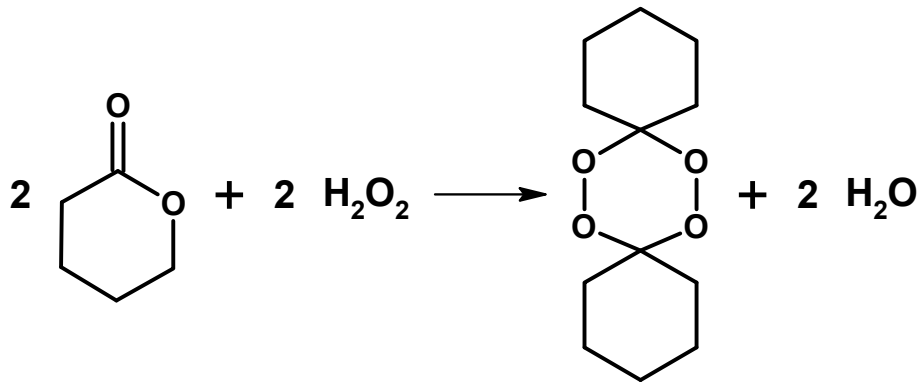

Figure 4. *First step of the Synthesis of Story: synthesis of dicyclohexylidene diperoxide via cyclohexanone oxidation using hydrogen peroxide and acid catalyst*

The scale-up of this reaction is difficult cause of its safety issues. High concentrated H_2O_2 is highly reactive and could lead to uncontrolled oxidations followed by a high generation of heat. A corrosive reaction mixture due to the presence of concentrated perchloric acid also increases the dangerousness of this reaction.

Many authors tried to improve the safety of the reaction and understand the better conditions to obtain selectively di or tri peroxide (Sanderson, *et al.*, 1975; Sanderson and Story, 1974).

A relevant contribution to achieve safer and applicable to industrial scale conditions for the first step of Story Synthesis was given by the research group directed by prof. Dr. Sempere, at IQS School of Engineering.

Among all, particularly important was the work of Avilés (2004). He optimised the synthesis of TCHP and DCHP and performed a safety analysis on the same reaction. Moreover, he developed a process to synthetize TCHP from cyclohexanone and 35 % concentrated hydrogen peroxide, using phosphotungstic acid as catalyst, a safer and less aggressive compound.

However, the reaction is still not completely suitable for large scale application.

A batch reactor in large scale is not safely possible, whereas a semi-batch operation is more appropriate, but highly reliable safety measures must be provided (Nomen *et al.*, 2003).

Since the reaction in batch was optimized, a Flow chemistry based reactor could be developed to continuously produce TCHP in a safe and industrially scalable way.

1.1.2 Macrolactones from cyclohexanone peroxides decomposition

The second step of the Story Synthesis basically consists of the thermal or photochemical decomposition of the previously synthetized cyclohexanone peroxides.
TCHP decomposition leads to the formation of 16-hexadecanolide (15-18 %) from the supposed reaction reported in Figure 5; cyclopentadecane (Figure 7, F) (28-34 %) and cyclohexanone are other two main products.
Yields in brackets are obtained at 180°C using different solvents. Changing the solvent does not quantitatively change the yield. Cyclopentadecane can be obtained in higher yield at higher temperatures, although 16-hexadecanolide's one is not significantly affected (Sanderson and Story, 1974).

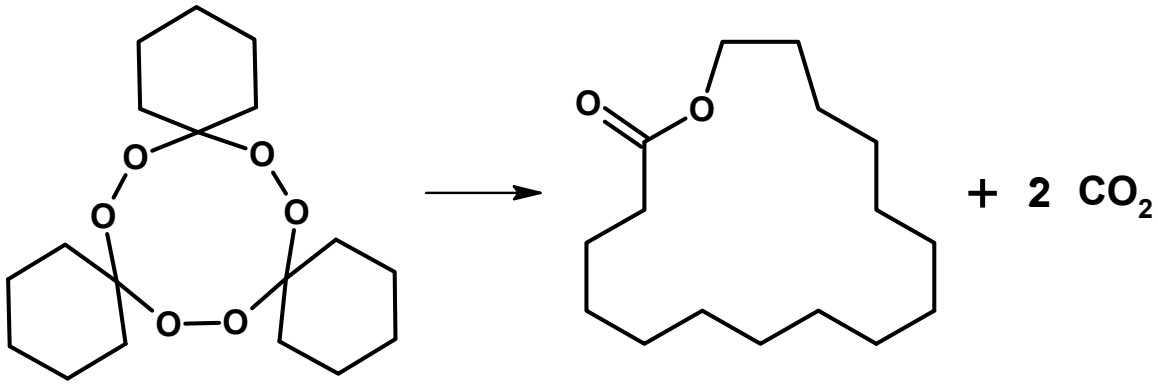

Figure 5. *Theoretical reaction of 16-hexadecanolide formation from TCHP decomposition. 2 moles of CO_2 are generated for each mole of TCHP reacted.*

Decomposing DCHP provides cyclodecane (Figure 7, E) (5-10 %), 11-undecanolide (Figure 7, A) (30-35 %) and cyclohexanone (5-10 %), at 160°C (Sanderson, 1974).
Different products can be obtained depending on which peroxides is decomposed. DCHP and TCHP can be functionalised to obtain substituted macrocyclic lactones and hydrocarbons (Bush and Story, 1970; Paul *et al.*, 1976).
The specific interest in TCHP decomposition comes from the possibility to obtain high value-added molecules in a rather easy way. 16-hexadecanolide has relevance in cosmetic industry because it is a basic element of musk aroma and it is a fixative for volatile fragrances; moreover, it shows good stability and smells good. DSC records reveal a first exothermic phenomenon at 340°C, due to its decomposition. Its stability is than verified for a wide range of temperatures (de Armas, 2015).
Musk aroma historically comes from animal source, but its large-scale need made mandatory the substitution for a synthetic one. Polycyclic compounds, like galaxolide (Figure 6, left), were

the first. Macrocyclic musk, like ambrettolide (Figure 6, right), became more attractive since their production is easier and less expensive.

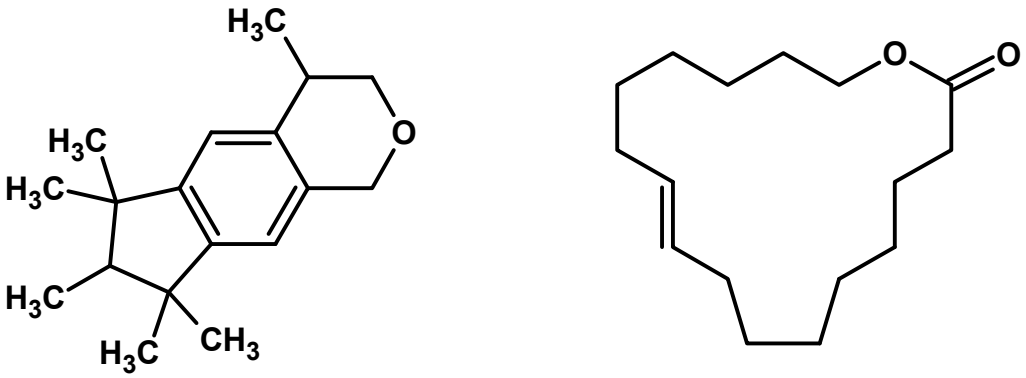

Figure 6. *Galaxolide on the left and ambrettolide on the right.*

At the moment, even though its inherent dangerousness, the synthetic route proposed by Story is the less expensive way to obtain macrocyclic compounds (Williams, 1999).
A detailed study on the TCHP decomposition to produce macrolactones was done by De Armas D. Ph.D. A chromatographic method to identify TCHP, DCHP and decomposition products was developed. Compounds of interest were identified and quantified using HPLC (de Armas, 2015). They are reported in Figure 7.

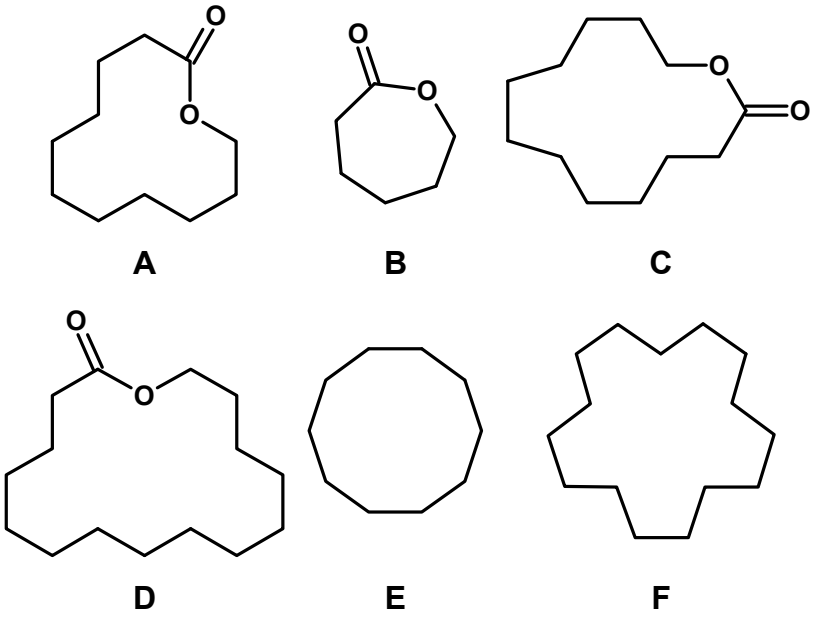

Figure 7. *Macrocyclic lactones and hydrocarbons. 11-undecanolide (A), 6-hexadecanolide (B), 12-dodecanolide (C), 15-pentadecanolide (D), cyclodecane (E), cyclopentadecane (F).*

The total yield in macrolactones was found to be equal to about 50 %. It comprises around 40 % of 16-hexadecanolide and 11-undecanolide (Figure 7, A) in equal proportion and around 10 % of 6-hexanolide (Figure 7, B). 12-dodecanolide (Figure 7, C) and 15-pentadecanolide (Figure *7*, D) were found in a negligible amount.
In addition, the effect of temperature, initial amount of reagent, reaction progress and solvent type on yield in 16-hexadecanolide was investigated. Conclusions are reported in Table 1.

Table 1. *Reaction conditions for TCHP decomposition to obtain high yield in macrolactones.*

Temperature / °C	Reaction time / min	TCHP concentration / w	Solvent
165-175	30-60	2-4 %	Decane or dodecane

In the following paragraph, it will be shown how flow chemistry techniques can help to improve the process safety and to make it applicable also to an industrial scale.

1.2 Flow chemistry techniques

1.2.1 Continuous manufacturing and fine chemicals industry

Termed batch chemistry is the traditional approach to perform organic synthesis. Even though it is well-known, it has remained based on the usual stirred round-bottom flasks. On the other hand, last decades have seen a huge development of continuous flow technologies, both on laboratory and industrial scale.
Continuous manufacturing provides some advantages with respect to batch production:

- Minimum manual handling
- Smaller equipment and facilities
- Robustness in product quality
- Reliable in-line monitoring and control (PAT)
- Faster response capability
- Intrinsic improvements on the process safety
- Processes operates at their optimum

Whereas petrochemical, polymer and bulk chemicals industries has been adopting continuous processes decades ago, pharmaceutical and fine chemical companies are still basing their production on stirred tank reactors.
An important step forward in this sense came from U.S: Food and Drug Administration (FDA). In 2004 they published a “Guidance for Industry” in which they introduced the concept of *quality by design*. It was a new way of thinking in contrast with traditional *a posteriori*

evaluation of quality. Process Analytical Technology (PAT) were promoted as a system to ensure it.

However, the implementation of continuous manufacturing has been slowed down by some barriers.

Firstly, FDA's guidance does not provide practical instructions about how to implement it, remaining in the scope of suggestions. Secondly, it is apparently more important to have a commercially ready product as soon as possible, instead of investing in innovative technologies to produce it. Thirdly, a general lack of experience in Flow chemistry from the managers of the fine chemistry industry.

In contrast, many authors developed flow process to carry out reactions related to pharmaceutical industry, improving safety, selectivity and the overall efficiency (Mason *et al.*, 2007; Seeberger *et al.*, 2009).

In the following paragraph will be described the advantages of performing the TCHP thermal decomposition using flow chemistry techniques.

1.2.2 The tube-in-tube reactor and its application to TCHP decomposition

The tube-in-reactor is a flow reactor made of two concentric tubes. The external tube is made of Teflon®, whereas the inner one is build using Teflon® AF-2400. It is an amorphous fluoropolymer of PDD (2,2-bistrifluoromethyl-4,5-difluoro-1,3-dioxole) and tetrafluoroethylene (TFE) (Figure 8).

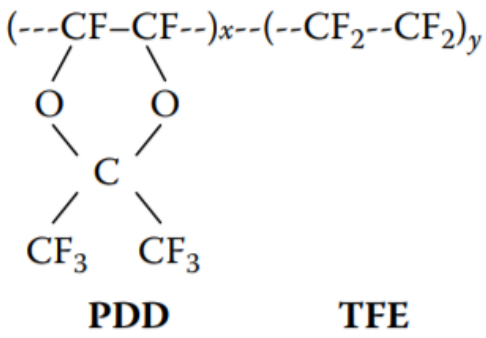

Figure 8. *Structure of Teflon® AF-2400.*

The resulting copolymer has the features of fluorinated polymers, like high temperature stability, excellent chemical resistance, low surface energy and low water absorption combined with the properties given by the completely amorphous structure: high optical transmission, solubility in perfluorinated solvents at room temperature, low refractive index, stiffness and high gas permeability (Resnick and Buck, 1997).

Given those unique properties of Teflon® AF-2400, the tube-in-tube reactor was widely used to carry out gas-liquid reactions, in order to enhance gas-liquid mixing at minimum gas usage. Its applicability was demonstrated by Brzozowsky *et. al* using many gaseous reagents, like CO, H_2, NH_3, O_2, CO_2, ethylene, syngas (1:1 CO/H_2) and dimethylamine.

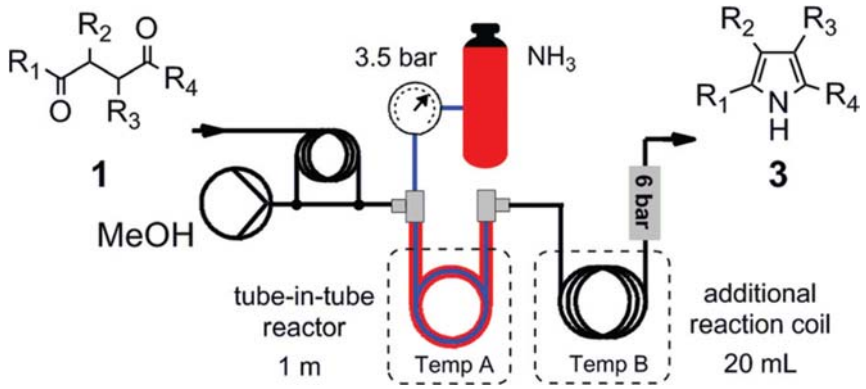

Figure 9. *Schematic of the flow apparatus used in the Paal-Knorr pyrrole synthesis.*

The same authors, for example, developed a system to perform the Paal-Knorr synthesis of pyrrole. A batch process is not suitable due to the high volatility of ammonia in liquid solution at reaction temperature (around 100°C). Liquid solutions were substituted by the diffusion and solubilisation of gaseous ammonia through the reactor membrane. The system is made of two pressurised coils. The first operates at low temperature (around 0°C) to enhance the absorption of NH_3, the second operate at the reaction temperature (Cranwell *et al.*, 2012).

The TCHP decomposition does not requires any gaseous reactant, but its extreme exothermicity is the crucial issue. TCHP is available as crystalline solid at ambient conditions (melting point: 88°C) and its thermal decomposition is usually carried out at temperatures greater than 150°C. It must be dissolved in a high boiling point organic solvent, like *n*-dodecane, to absorb the heat of reaction. The 4 % w/w solution show a heat of reaction equal to - 2333±40 $J \cdot g^{-1}$: a batch reactor is not a safe alternative to perform the reaction, not even at high dilution (Ferrer *et al.*, 2018). In any way, a discontinuous jacketed reactor does not allow to ensure a cooling system able to counteract a reaction runaway.

Flow reactors offer the possibility to reduce the volumes of reactant and increase the surface available to disperse the heat of reaction. The internal diameter of the tubular reactor made of Teflon® AF-2400 is usually smaller than 1 mm and the total volume of the reactor is in the order of magnitude of millilitres.

The second advantage of tube-in-tube reactor is the possibility to extract the gaseous products (CO_2) produced during the TCHP decomposition. Using a simple PTFE tubular reactor, the generation of CO_2 gives rise to a gas-liquid system, characterised by an unpredictable behaviour. For example, if an unpredicted temperature rise of the heating bath occurs, reaction

rate is made faster and CO_2 is sudden released. At high temperature it expands and could provoke tubing collapse or, at the best, could rapidly push 170° *n*-dodecane out of the reactor.

Chapter 2

Thermal analysis of tricyclohexylidene triperoxide decomposition

In this chapter it is explained how the kinetic model of TCHP thermal decomposition is obtained from thermal analysis techniques. Starting from an overview of thermal analysis technique, a brief presentation of NPK method is reported. An explanation of its application to autocatalytic reactions follows. The kinetic law of TCHP thermal decomposition is then reported at the end of the chapter.

2.1 Thermal analysis and calorimetry

Kinetic analysis of thermal analysis and calorimetry data is a basic tool to develop materials and processes. Usually it is assumed that in one process there is only one reaction rate controlling step, for which it is possible to express conversion (α) with the following equation:

$$\frac{\mathrm{d}\alpha}{\mathrm{d}t} = \Phi(\alpha, T, p)\ . \qquad \text{Eq. 1}$$

Reaction rate can be a more or less complex function of conversion, temperature (T) and pressure (p).

Most of the existent kinetic methods are based on the possibility to separate the functionality in three different independent functions, each one depending only on one variable. Since most of thermal analysis experiments are done at constant pressure, the functionality of pressure is constant and does not affect the reaction rate.

$$\frac{\mathrm{d}\alpha}{\mathrm{d}t} = \mathrm{g}(\alpha)\cdot \mathrm{f}(T)\cdot \mathrm{h}(p) \xrightarrow{p=\cos t} \frac{\mathrm{d}\alpha}{\mathrm{d}t} = \mathrm{g}(\alpha)\cdot \mathrm{f}(T) \qquad \text{Eq. 2}$$

g(α), f(T) and h(p) represent the kinetic model of the process, the pressure and temperature dependence of the reaction rate respectively.

For the most common methods the functionality of temperature can be expressed using Arrhenius law:

$$f(T) = A \cdot e^{\frac{-E_a}{RT}}, \qquad \text{Eq. 3}$$

where A is the pre-exponential factor, E_a is the activation energy, R is the gas constant and T is the temperature.

Table 2 *Standard kinetic models*

Model	Notation	g(α)
Reaction's order model		
0^{th} order reaction	RO (0)	1
1^{st} order reaction	RO (1)	$(1-\alpha)$
n^{th} order reaction	RO (n)	$(1-\alpha)^n$
Accelerated models		
Potential	Pn	$n \cdot \alpha^{\frac{(n-1)}{n}}$
Exponential	En	α^n
Decelerated models		
Cylindrical contraction	R2	$2 \cdot (1-\alpha)^{1/2}$
Spherical contraction	R3	$3 \cdot (1-\alpha)^{2/3}$
One-dimensional diffusion	D1	$\frac{1}{2} \cdot \alpha^{-1}$
Two-dimensional diffusion	D2	$[-\ln(1-\alpha)]^{-1}$
Three-dimensional diffusion (Jander)	D3	$\frac{3}{2} \cdot (1-\alpha)^{2/3} \cdot \left[1-(1-\alpha)^{1/3}\right]^{-1}$
Three-dimensional diffusion (Ginstling-Brounshtein)	D4	$\frac{3}{2} \cdot \left[(1-\alpha)^{-1/3}-1\right]^{-1}$
Sigmoidal models		
Avrami-Erofeev	An	$n \cdot (1-\alpha) \cdot [-\ln(1-\alpha)]^{(n-1)/n}$
Prout-Tompkins	PT	$\alpha \cdot (1-\alpha)$
General models		
Truncated Sěsták-Berggren	SB(m,n)	$\alpha^m \cdot (1-\alpha)^n$
Sěsták-Berggren	SB(m,n,p)	$\alpha^m \cdot (1-\alpha)^n \cdot [-\ln(1-\alpha)]^p$

The functionality of conversion can be expressed using the Standard models, applicable to a lot of different processes (Table 2). All those kinetic laws are based on solid state chemistry and physics, even though other ones fit homogeneous chemical reaction perfectly (RO and PT).
h(p) can be considered when pressure of the system is not constant specially if the partial pressure of one of the products could affect the equilibrium of the system. However, if the gases formed can be rid of in a fast way these phenomena do not happen.

2.2 Typical kinetic analysis methods

The simplest kinetics analysis methods are the ones that use only one thermal analysis record to evaluate the parameters.
Usually they start assuming a n^{th}-order kinetic model (RO) and follow determining E_a, A and n, called kinetic triplet. The most common models of this type are multilinear regression and the method of Freeman-Carroll (Freeman and Carroll, 1958). The disadvantage of both two methods is that the kinetic triplet is always an apparent one, cause of the compensation effect and the n^{th}-order kinetic law assumption.
Finding more flexible parameters needs more than one record. All the following methods are based on three to five dynamic records of the same phenomena, changing the heating rate β.
The most important ones are:

- Method of the height of the peak (Kaiser and Ticmanis, 1995)
- Method of Flynn-Wall (Flynn and Wall, 1966)
- Method of Kissinger (Kissinger, 1957)

The method of the height of the peak is nowadays disused, but the Ozawa and Kissinger methods have been used widely to estimate activation energy.
More advanced methods are based on many regressions for different points of the records at the same conversion. They are called isoconversional methods. The main advantage of those methods is that they are capable to get the variation of the apparent activation energy while the reaction is proceeding, calculating it at different conversions. Previous methods just give one apparent activation energy mediated on the whole process. The most important are:

- Method of Friedman(Friedman, 1964)
- Method of Ozawa (Ozawa, 1965)
- Method of Kissinger-Akahira-Sunose (Akahira and Sunose, 1971)
- Free Model (Vyazovkin and Dollimore, 1996).

2.3 Non-Parametric Kinetics method

Non-Parametric Kinetics method (NPK) was developed for the first time in 1998 at the Chemical Engineering Department of IQS School of Engineering (Serra *et al.*, 1998a and 1998b) and successively extended (Sempere *et al.*, 1999, 2002).

NPK method is capable of separating the two functions g(α) and f(*T*) of Eq. 2. The innovation of NPK is that it does not assume any kinetic model, not even the Arrhenius law.

NPK method starts from the experimental data matrix, called **A**. It is a surface where each point is the reaction rate for a specific pair of conversion and temperature.

$$\mathbf{A}_{n\times m} = \begin{pmatrix} \left(\frac{\mathrm{d}\alpha}{\mathrm{d}t}\right)_{1,1} & & \\ & \cdots & \\ & & \left(\frac{\mathrm{d}\alpha}{\mathrm{d}t}\right)_{n,m} \end{pmatrix} \qquad \text{Eq. 4}$$

It is assumed that this matrix comes from the multiplication of two vectors:

$$\mathbf{A} = \mathbf{g}\cdot\mathbf{f}^{T}, \qquad \text{Eq. 5}$$

where vectors **g** and **f** are defined as:

$$\mathbf{g} = \begin{pmatrix}\mathbf{g}(\alpha_1) & \mathbf{g}(\alpha_2) & \cdots & \mathbf{g}(\alpha_n)\end{pmatrix}^{T} \qquad \text{Eq. 6}$$

$$\mathbf{f} = \begin{pmatrix}\mathbf{f}(T_1) & \mathbf{f}(T_2) & \cdots & \mathbf{f}(T_m)\end{pmatrix}^{T}. \qquad \text{Eq. 7}$$

Then, the following is obtained:

$$\mathbf{A}_{n\times m} = \begin{pmatrix} \mathbf{g}(\alpha_1)\cdot\mathbf{f}(T_1) & \mathbf{g}(\alpha_1)\cdot\mathbf{f}(T_2) & \cdots & \mathbf{g}(\alpha_1)\cdot\mathbf{f}(T_m) \\ \mathbf{g}(\alpha_2)\cdot\mathbf{f}(T_1) & \mathbf{g}(\alpha_2)\cdot\mathbf{f}(T_2) & \cdots & \mathbf{g}(\alpha_2)\cdot\mathbf{f}(T_m) \\ \vdots & \vdots & \ddots & \vdots \\ \mathbf{g}(\alpha_n)\cdot\mathbf{f}(T_1) & \mathbf{g}(\alpha_n)\cdot\mathbf{f}(T_2) & \cdots & \mathbf{g}(\alpha_n)\cdot\mathbf{f}(T_m) \end{pmatrix} \qquad \text{Eq. 8}$$

The decomposition of **A** matrix in the product of two vectors **g** and **f** is done using the principal component analysis; in particular, the singular value decomposition:

$$\mathbf{A} = \mathbf{U}\cdot\mathbf{W}\cdot\mathbf{V}^{T} \qquad \text{Eq. 9}$$

In that way, **A** matrix is obtained as the product of three matrices. The dimension of those ones can vary depending on the algorithm used to decompose the original one. MATLAB® provides the *svd* algorithm that gives results in the following form:

$$\mathbf{A}_{n\times m} = \mathbf{U}_{n\times n} \cdot \mathbf{W}_{n\times m} \cdot \mathbf{V}^{T}_{m\times m} \qquad \text{Eq. 10}$$

Each $\mathbf{u_i}$ column of **U** matrix includes the information from the conversion functionality g(α). Similarly, each column $\mathbf{v_i}$ of **V** matrix includes the information from the temperature functionality f(T). **W** is a diagonal matrix, containing the decomposition singular values, sorted in decreasing order in a way that:

$$\forall i \le \min(n,m) \Rightarrow w_{i+1} \le w_i \qquad \text{Eq. 11}$$

The number of significant singular values is important because it says how many pairs of **u**-**v** vectors are significant to describe correctly the experimental data contained in **A** matrix.
If the transformation is dominated by only one rate-determining process, then it will occur that $w_1 >> w_2 \approx 0$. For this reason, **A** matrix can be approximated just by the first two vectors of **U** and **V** matrices:

$$\mathbf{A} \cong \vec{\mathbf{u}}_1 \cdot w_1 \cdot \vec{\mathbf{v}}_1^{T} \text{''} \qquad \text{Eq. 12}$$

Those two significant vectors are proportional to the **g** and **f** original ones. Real functionalities can be easily obtained determining the a and b scalars:

$$\mathbf{g} = a \cdot \vec{\mathbf{u}}_1 \qquad \text{Eq. 13}$$

$$\mathbf{f} = b \cdot \vec{\mathbf{v}}_1 \qquad \text{Eq. 14}$$

At the same time, it has to accomplish that:

$$a \cdot b = w_1 \qquad \text{Eq. 15}$$

Once this functionality is known, it is possible to assign a model to each vector. The most common models for **u** vector are the ones listed in Table 2, whereas the most typical one for **v** vector is Arrhenius law. When the model is chosen, its kinetic parameters can be found by regression.

2.4 Autocatalytic reactions

One limitation of thermal analysis techniques like Differential Scanning Calorimetry or Thermogravimetric Analysis is that they provide one single signal, such as heat flow, mass…, even if there is more than one process occurring. Therefore, it is possible to calculate just one global conversion considering all the single phenomena that can appear during an experiment.

In some cases, it is possible to distinguish among different processes, but they need to occur at sufficiently separated temperatures providing two sufficiently separated signals, or they have to produce a different kind of signal, *e.g.* one loses mass, the other only generates heat.
Parallel reactions

$$\begin{aligned} A &\rightarrow B \\ A &\rightarrow C \end{aligned} \qquad \text{Eq. 16}$$

and consecutive reactions

$$A \rightarrow B \rightarrow C \qquad \text{Eq. 17}$$

are an example of transformations made of more than one reaction that generally provide experimental signals in the same temperature interval. In these conditions, thermal analysis techniques are not useful to calculate the rate of one single reaction.
On the other hand, autocatalytic reactions can be described by the following single chemical equation:

$$A + B \rightarrow 2B\ . \qquad \text{Eq. 18}$$

Starting from that, thermal analysis can provide a kinetic low giving rise a single representative conversion.
The general feature of autocatalytic reactions is that their reaction rate increases while the transformation is proceeding.
Traditionally, kinetic laws of autocatalytic reactions can be satisfactory described using a Prout-Tompkins model or a more general Šesták Berggren model, reported in Eq. 19 and in Eq. 20 respectively. Temperature functionality usually is assumed to be expressed by Arrhenius law.

$$\frac{\mathrm{d}\,\alpha}{\mathrm{d}\,t} = k \cdot \alpha \cdot (1 - \alpha) \qquad \text{Eq. 19}$$

$$\frac{\mathrm{d}\,\alpha}{\mathrm{d}\,t} = k \cdot \alpha^{m} \cdot (1 - \alpha)^{n} \qquad \text{Eq. 20}$$

Even though experimental data can be correctly reproduced using one of the previous models, the reaction rate is zero when α is zero, making the numerical simulation unrealisable. Assuming an initial non-zero conversion leads to a situation in which changing the initial value, changes the shape of the predicted DSC curve.
In Figure 10 a truncated SB model has been simulated using different values of initial conversion. It is possible to observe that initial value of conversion has a considerable influence in estimating the induction time of the reaction.

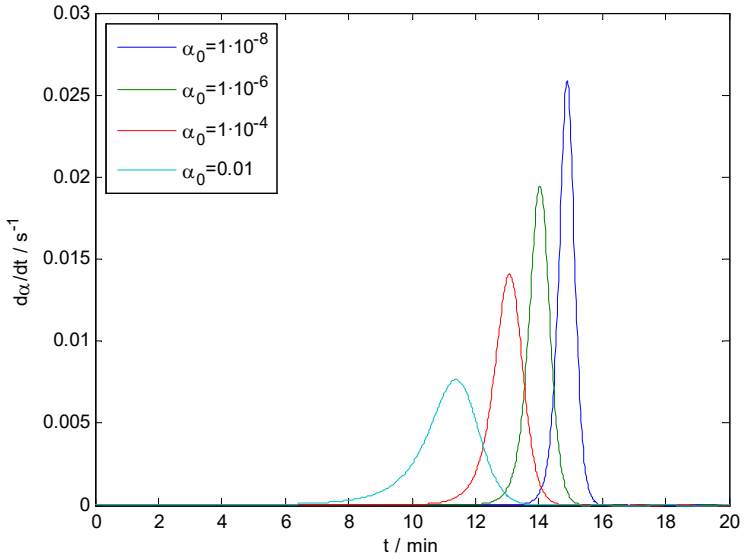

Figure 10. *SB model simulation using initial conversions of 10^{-8}, 10^{-6}, 10^{-4} and 10^{-2}. Parameters are: $A=3\cdot10^{9}\ s^{-1}$, $E_a=150\ kJ\cdot mol^{-1}$, $m=n=1$, $T_0=600\ K$ and $\beta=10\ K\cdot min^{-1}$.*

Induction period is a key parameter, because it gives an indication about the actual interval time before the reaction became observable in a macroscopic point of view. In Eq. 19, compound *B* is both a reagent and a product of the reaction of *A*. It cannot occur unless a certain amount of *B* is already available as reactant. This condition is usually provided by thermal activation of the reaction, according to the basic transformation: $A \rightarrow B$.

At some point, the rate of the autocatalytic mechanism of Eq. 19 is such that the activation reaction is minor and the process is self-sustained and self-accelerated. The induction period is defined as the time needed to the reaction rate to be higher than a fixed-temperature estimated threshold. Since autocatalytic reactions are usually exothermic or strongly exothermic, like TCHP decomposition, that threshold has to be strictly related to the conditions to operate the process safely. The induction period is useful, for example, to have an estimation of the time available to start the emergency plan before a runaway occurs.

Correctly simulating the induction period requires the development of two simultaneous processes models. J. Dien *et al.* (1994) applied a combination of a first order and a SB model to simulate the initiation and the autocatalytic part respectively.

$$\frac{\mathrm{d}\,\alpha}{\mathrm{d}\,t} = k_1 \cdot (1-\alpha) + k_2 \cdot \alpha^{m} \cdot (1-\alpha)^{n} . \qquad \text{Eq. 21}$$

In terms of chemical equations, it is represented by the following system:

$$\begin{matrix} A \rightarrow B \\ A + B \rightarrow 2\,B \end{matrix} , \qquad \text{Eq. 22}$$

which is thermodynamically equivalent to $A \rightarrow B$. Therefore, a unique value of conversion α is theoretically correct.

In previous works, Ferrer *et al.* (2017) applied NPK method to autocatalytic processes concluding that experimental data reconstruction can be done using only the first pair of vectors ($\mathbf{u_1}$ and $\mathbf{v_1}$). Then, the kinetic law contains only one functionality of temperature, *i.e.* only one kinetic constant. In the same work it is confirmed that a first order model and a truncated Šesták-Berggren equation appropriately describe an autocatalytic reaction.

The final model proposed is the following:

$$\frac{\mathrm{d}\,\alpha}{\mathrm{d}\,t} = A \cdot e^{-E_a/(R \cdot T)} \cdot \left[\gamma(1-\alpha) + \cdot\alpha^m \cdot (1-\alpha)^n\right] \cdot \qquad \text{Eq. 23}$$

The main difference from Eq. 21 is that NPK method can provide only one value of activation energy, making the two supposed processes of Eq. 22 indistinguishable from a modelling point of view. However, γ represents the relative weight of the autocatalytic reaction with respect to the initiation (RO) reaction.

It is also demonstrated that Eq. 23 is capable to correctly predict the induction time of several autocatalytic processes, overcoming the compensation effect of the previous methods.

In the following paragraph it will be shown how the kinetic of TCHP decomposition is obtained applying this method to DSC experimental data.

2.5 Kinetic law of TCHP thermal decomposition

Ferrer *et al.* (2018) studied the thermal decomposition of TCHP applying the NPK method with the adaptation to autocatalytic processes proposed by the same authors and described in the previous paragraph. Experimental data were obtained from DSC records:

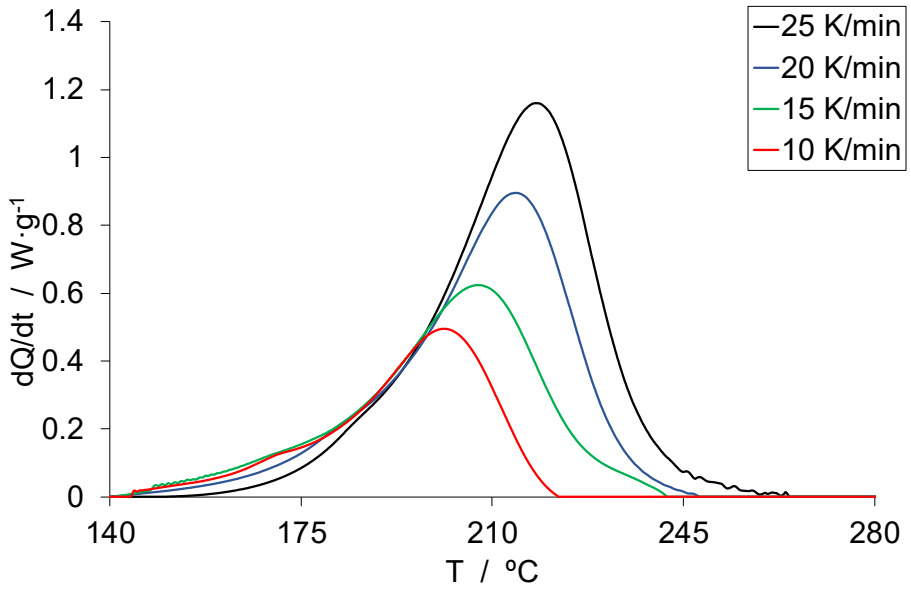

Figure 11. *Kinetic study of 4% solution TCHP decomposition. DSC experiments at different heating rate: 25, 20, 15 and 19 K·min^{-1} using stainless steel crucible in the temperature interval of 30-300°C.*

The kinetic law was studied for pure TCHP and for its 4 % w/w solution in *n*-dodecane. For the second case, DSC experiments were performed in medium pressure crucible, to avoid solvent evaporation (Figure 11).

A first order equation and a Šesták-Berggren model are adjusted. Eq. 23 is applied.

The results of the kinetic analysis and the heat of reactions are reported in the following table:

Table 3. *Kinetic parameters and heat of reaction for the thermal decomposition of pure TCHP and its 4 % w/w solution.*

TCHP	A / s^{-1}	E_a / kJ·mol^{-1}	γ / -	m / -	n / -	ΔH_R / J·g^{-1}
Pure	$9.60 \cdot 10^{14}$	148.2±0.8	0.092	0.283	1.165	- 1972±38
4% w/w solution	$1.97\ 10^{8}$	90.9±0.8	0.228	0.853	1.405	- 2333±40

The enthalpy of reaction changes when the reactant is pure TCHP or its 4 % w/w solution. The authors suggest that this change is due to a modification of the mechanism of the reaction itself, having excluded other possibilities.

The values of second line of Table 3 are used in this work every time it is required to simulate the reaction rate of TCHP thermal decomposition.

Chapter 3

Synthesis and batch decomposition of tricyclohexylidene triperoxide

In the first part of this Chapter the results of the synthesis of tricyclohexylidene triperoxide are shown. The synthetic route of this compound is rather difficult, and guidelines provided by literature need to be carefully followed.
The Chapter follows with the explanation of the construction of the TCHP decomposition design of experiment and it is concluded with the identification of the conditions at which the continuous process is carried on.

3.1 Synthesis of TCHP

Tricyclohexylidene triperoxide is obtained from the procedure developed by Nomen *et al.* (2003). They provide an easy and safe method to carry out the first step of the Synthesis of Story. More details about the experimental procedure can be found in the Ph.D thesis of Dr. K. Avilés (Avilés, 2004) and in the Thesis of R. Villa (Villa, 1999).
Three batches of TCHP are produced following the procedure described in §5.4. The second one is wasted because a sudden and uncontrolled temperature rise led to the formation of an unidentified sticky substance from which it was impossible to extract the phase containing the peroxide.
The other two batches are named Batch 1 and Batch 2 and both end white a crystalline solid as final product, with a yield of 18.2 % and 23.2 %, calculated using Eq. 24.

$$Y = \frac{n_{TCHP}^{eff}}{n_{TCHP}^{th}} \cdot 100 \,, \qquad \text{Eq. 24}$$

n_{TCHP}^{eff} are the moles of the TCHP actually recovered and weighted and n_{TCHP}^{th} are the theoretical moles of TCHP assuming total conversion and taking into account the reaction mentioned in Figure 3.
Dr. K. Avilés obtained a yield of 46.9 % at the same conditions used in this work.
Those yields are lower than the previous reported ones and this is mainly due to two reasons.

The first one is the absence of an automatic temperature regulation, that leads to an inaccurate control of this crucial variable. Yield of 36.9 % and 22.8 % were obtained at 65°C and 75°C in slightly different reagent to catalyst ratio ($g_{PA.}/g_{CHX} = 0.03$; $mol_{CHX}/mol_{H_2O_2} = 1.1$). A temperature change of 10°C reduces the yield of almost 40 %.
The second one is the loss of some TCHP in the wasted aqueous phase.
Both issues can be easily solved improving the equipment and separation operations, to correctly reproduce literature results.
The characterization of Batch 1 and Batch 2 TCHP is done via DSC and HPLC, according to the procedure described in §5.3.2.
The complete DSC records can be found in Figure 12.

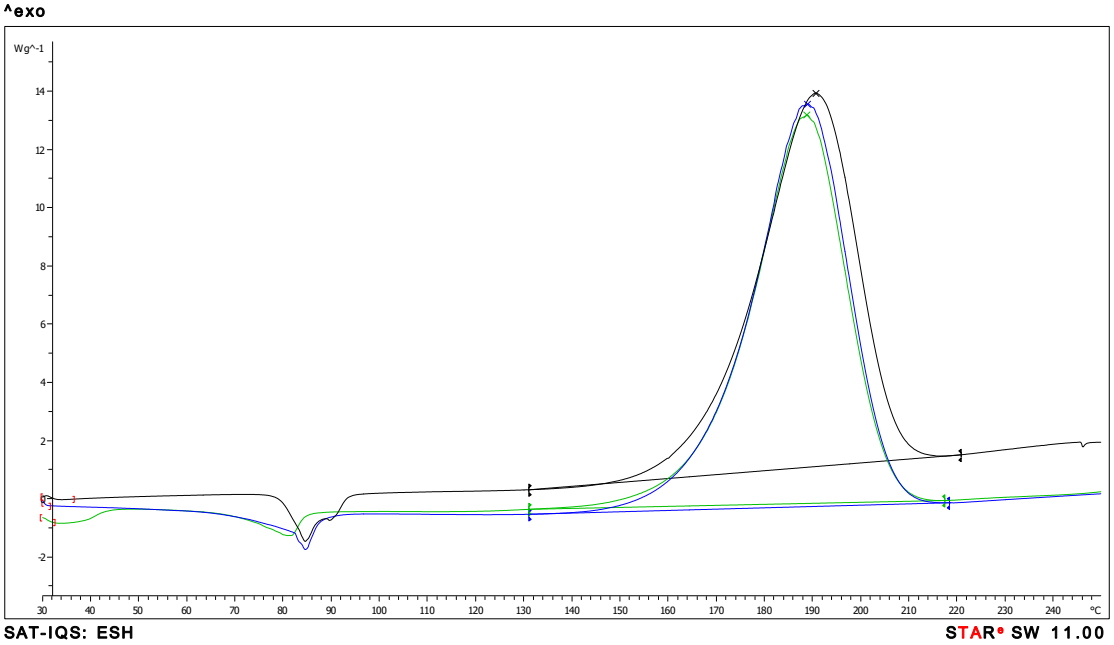

Figure 12. *Raw DSC records of Reference (black line), Batch 1 (blue line) and Batch 2 (green line) TCHP. Samples are prepared in a 70 µl standard crucible of aluminum, β=10 K·min^{-1}, temperature interval between 30 and 250°C, N_2 flowrate of 50 ml·min^{-1}.*

A first look at those records shows that there are mainly two peaks: the first one due to an endothermic phenomenon, associable to the melting of THCP; the second one to an exothermic one, corresponding to its decomposition. From the former, two quantitative information can be extracted: its onset temperature and heat of decomposition.
Batch 1 and Batch 2 are compared to a Reference TCHP and to values provided by literature (Ferrer *et al.*, 2018). Reference TCHP is provided by Dr D. de Armas, characterised via HPLC, DSC and IR and declared to be 99% pure (de Armas, 2015). In Figure 13 are shown the peaks corresponding to the thermal decomposition of TCHP.

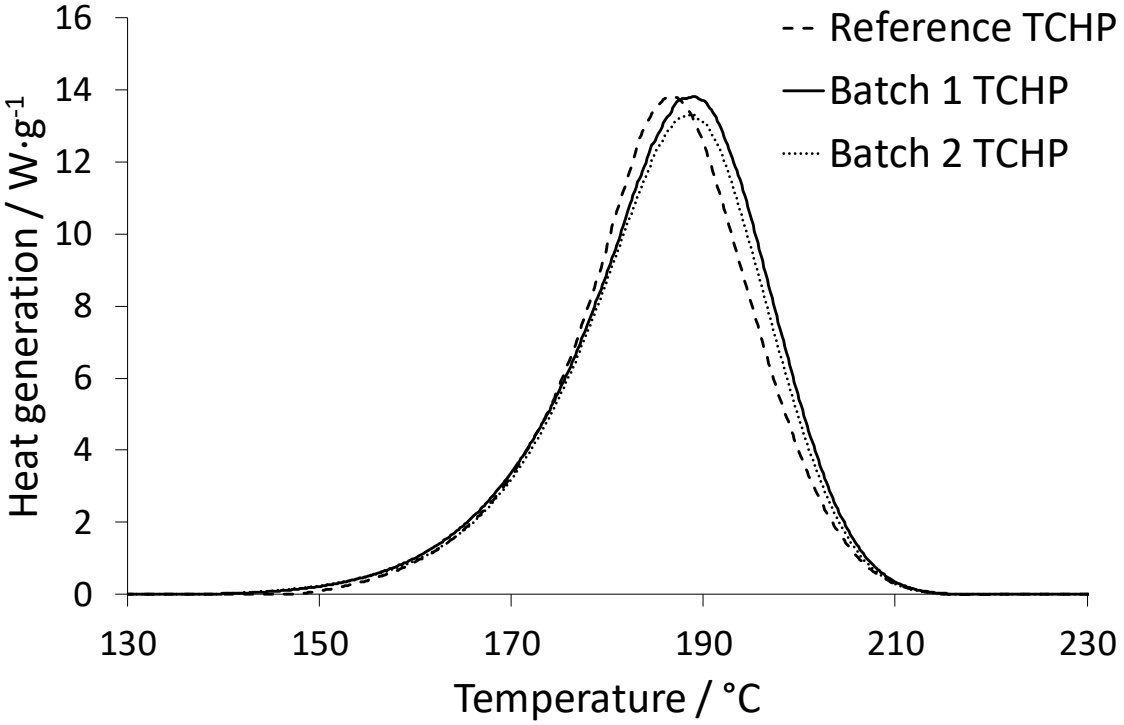

Figure 13. *DSC records of Reference, Batch 1 and Batch 2 TCHP. Samples are prepared in a 70 µl standard crucible of aluminum, β=10 K·min^{-1}, temperature interval between 30 and 250°C, N_2 flowrate of 50 ml·min^{-1}.*

Table 4 summarizes the values on which the comparison is based. "Reference", "Batch 1" and "Batch 2" columns of Table 4 are extracted from the plot of Figure 14.

Table 4 *Results of the DSC characterization of Reference, Batch 1 and Batch 2 TCHP. Literature values are taken from Ferrer et al. (2018.).*

Property	Literature	Reference	Batch 1	Batch 2
Heat of decomposition /kJ·kg^{-1}	1972 ± 38	1861	1985	1888
Onset Temperature /°C	-	168.7	170	169.1

The closeness of Onset Temperatures ensure that the same thermodynamics events are compared.

It has to be noticed that literature value comes from a work whose aim was to identify the kinetic law of TCHP decomposition and not specifically calculate the thermodynamic property taken into account. In that case, a larger number of samples would have been taken into account in order to obtain a reliable error margin. However, if the literature value is taken as the more reliable one, the following conclusions can be done.

Heats of decomposition of Reference, Batch 1 and Batch 2 TCHP are 5.6 % lower, 0.7 % higher and 4.3 % lower than the value provided by literature. Only the value obtained from Batch 1 is

included inside the confidence interval. The deviation of Batch 2 TCHP heat of decomposition can be due to the presence of small traces of methanol in the final product. Its evaporation can be observed in the interval of temperatures between 30 and 50°C.
Considering the percentage deviations calculated above and the declared purity of Reference, it is possible to conclude that the deviations are low enough to consider the Batch 1 and Batch 2 TCHP with a high purity.
Another aspect to be considered is that one of the main impurities that can be generated during the synthesis of TCHP is the DCHP and it can be difficult to observe it just looking at the heat of decomposition. It is important to reduce as much as possible the presence of DCHP inside TCHP, because the final yield in 16-hexadecanolide can be reduced by the formation of lower molecular weight cyclic macrolactones (Figure 7) (de Armas, 2015).
In Figure 14 it is shown a DSC record of DCHP, realised as described in §5.3.1.

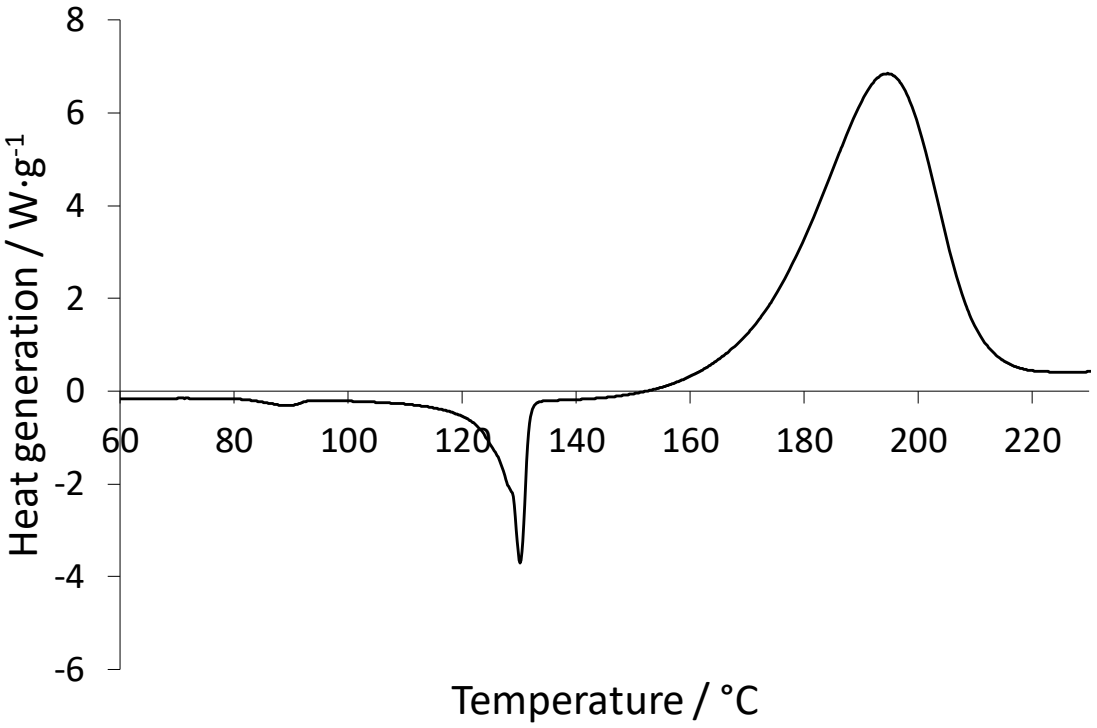

Figure 14. *DSC record of DCHP. Sample is held in a 70 µl standard crucible of aluminium. β=10 K·min^{-1}, temperature interval between 30 and 250°C, nitrogen flowrate of 50 ml·min^{-1}.*

Thermal decompositions of DCHP and TCHP occur around the same interval of temperatures, for a given heating rate. Indeed, an onset temperature of 169.9°C is found.
What really distinguish those two compounds is their respective melting point. TCHP melting point is placed around 88°C, whereas melting point of 127.4°C is obtained from the plot in Figure 14. DSC records of TCHP don't show any peak in that temperature interval.
This observation allows to conclude that the presence of DCHP can be neglected.

Batch 1 and Batch 2 are further analysed via HPLC according to the method described in §5.3.2. Figure 15 shows the three chromatograms overlapped and subtracted the blank.

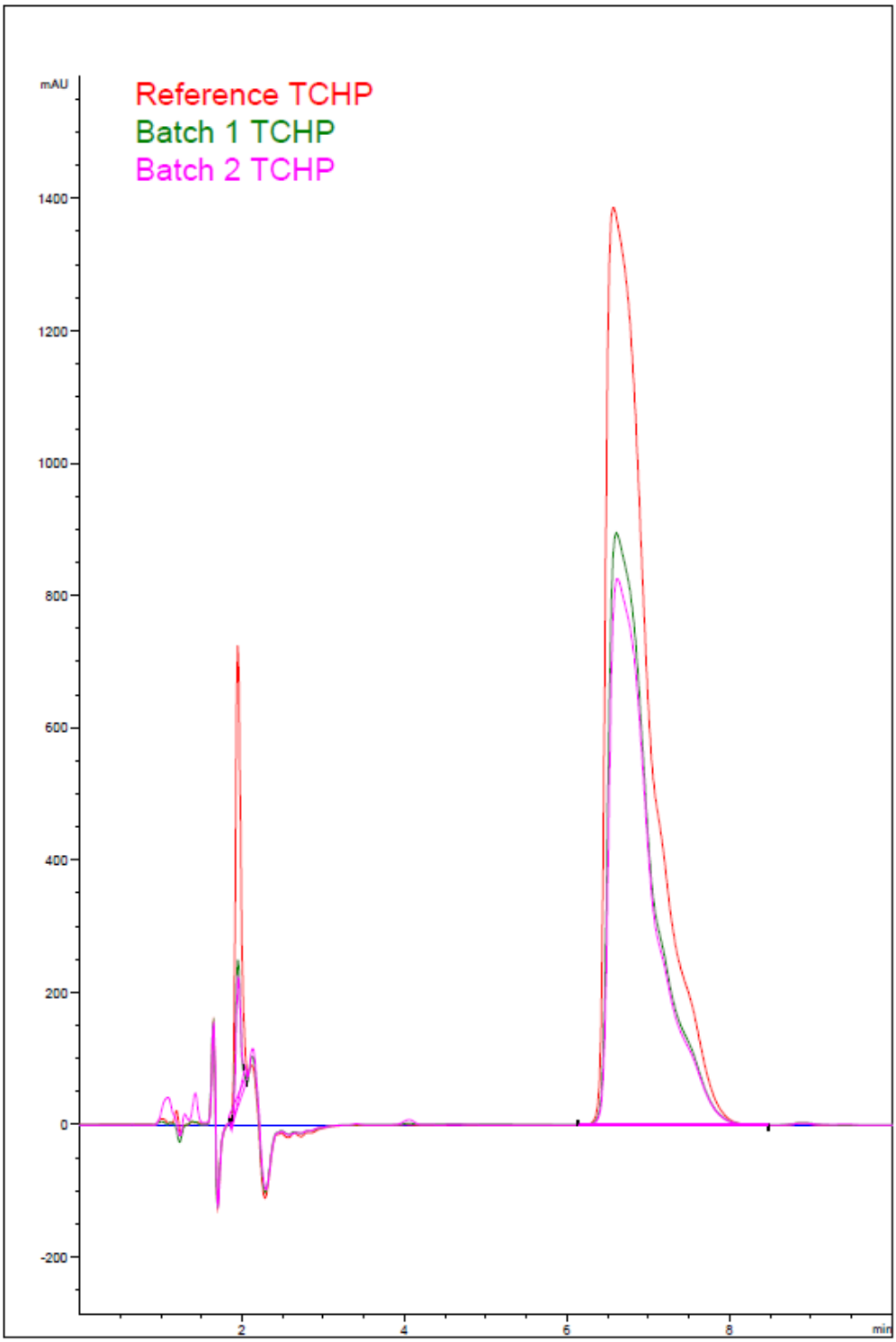

Figure 15. *HPLC chromatograms of Batch 1, Batch 2 and Reference TCHP subtracting blank (n-dodecane) chromatogram. Stationary phase: Nova-Pak® C18 column; mobile phase: acetonitrile / water (90:10 v/v), flowrate of 1 ml·min^{-1}, wavelength of 210 nm.*

Table 5 summarises information extracted from Figure 15.

Table 5. *Retention time and chromatographic purity of Reference, Batch 1 and Batch 2 TCHP.*

TCHP	Retention time / min	Chromatographic purity
Reference	6.57	94.4 %
Batch 1	6.61	97.1 %
Batch 2	6.62	97.5 %

The expected retention time for TCHP is 6.6±0.1 min. The three chromatograms are totally similar, with the peak of TCHP in the expected position, the difference in the areas of the peaks is due to the different amount of TCHP contained in each sample.
Retention factor is calculated from literature chromatograms (de Armas, 2015). The position of DCHP's peak is identified and its area its calculated by integration of the curve.
Chromatographic purity is calculated as the percentage fraction of the integral of the TCHP peak with respect to the sum of the integrals of all the other detectable peaks, *i.e.* the peak of DCHP. Indeed, all the other peaks can be treated as traces of impurities and neglected in the determination of the purity of Batch 1 and Batch 2.
It has to be noticed that chromatography purity is a reliable parameter if it is assumed that DCHP and TCHP has the same molar absorptivity, at the wavelength at which the detector operates.
The two molecules differ from an oxygen single bond and a cyclohexyl group. The absorbance of a molecule is not significantly affected by the presence of those groups. For this reason, the assumption holds. However, chromatographic purity is a sufficient indicator for the basic evaluation needed for the aim of this work.
In the light of above, there enough reasons to neglect any difference between the Reference TCHP and the one of Batch 1 and Batch 2.

3.2 Thermal decomposition of TCHP

The aim of those experiments is to explore the general features of the TCHP thermal decomposition, investigating the effect of reaction time, mass fraction of reagent and temperature on conversion, selectivity and yield.

3.2.1 Construction of Taguchi matrix

The design of experiment is based on modified orthogonal Taguchi matrix, build as follow:
Response variables are supposed to be influenced by three factors (A, B and C). A and B factors are arranged on two levels, C factor on three.

A four degrees of freedom Taguchi matrix is needed to assign all those factors. $L_8(2^7)$ Taguchi matrix (Table 6) has at the same time the less number of required experiments and columns enough (7) to fulfils four degrees of freedom. However, this matrix does not directly allow to assign a three level factor. A combination of columns is needed.

Table 6. *$L_8(2^7)$ Taguchi matrix.*

	1	**2**	**3**	**4**	**5**	**6**	**7**
1	1	1	1	1	1	1	1
2	1	1	1	2	2	2	2
3	1	2	2	1	1	2	2
4	1	2	2	2	2	1	1
5	2	1	2	1	2	1	2
6	2	1	2	2	1	2	1
7	2	2	1	1	2	2	1
8	2	2	1	2	1	1	2

Columns 6 and 7 are combined to obtain a three levels column, following the combinatory shown in Table 7:

Table 7. *Combination of column 6 and column 7.*

Col. 6	**Col. 7**	**Col. 6+7**
1	1	1
1	2	2
2	1	2
2	2	3

This modification produces a $L_8(2^5x3^1)$ matrix (Table 8) which presents a loss of orthogonality of 12.5 % due to a higher importance given to the medium level of C factor. This loss is calculated with respect to the original Taguchi matrix and it is assumed acceptable.

Table 8. *$L_8(2^5x3^1)$ Taguchi matrix.*

	1	**2**	**3**	**4**	**5**	**6**
1	1	1	1	1	1	1
2	1	1	1	2	2	3
3	1	2	2	1	1	3
4	1	2	2	2	2	1
5	2	1	2	1	2	2
6	2	1	2	2	1	2
7	2	2	1	1	2	2
8	2	2	1	2	1	2

To assign the three factors, A, B and C factors are placed on three different columns. The remaining ones are filled with AxB and BxC interactions. One column is required for the first one, whereas the second one is split in two columns. AxC interaction is confused within C factor.
The assignation is resumed in the following alias structure (Table 9).

Table 9. *Alias structure.*

Column	Main effect	Confusion
1	A	
2	B	
3	AxB	
4	1/2 BxC	
5	1/2 BxC	
6	C	+AxC

The final matrix is shown in Table 10.

Table 10. *Final experimental matrix*

	A	B	C
1	Low	Low	Low
2	Low	Low	High
3	Low	High	High
4	Low	High	Low
5	High	Low	Medium
6	High	Low	Medium
7	High	High	Medium
8	High	High	Medium

The effect of the different factors is analysed through Pareto's ANOVA, when the experimental data collection is completed.
Columns explaining together at least 95 % of variability are assumed the ones of higher effect. The remaining ones are treated as experimental error.

3.2.2 Design of experiment results

The design of experiment is developed starting from Table 10.
Variables are assigned to factors: reaction time to A, mass fraction of TCHP to B and temperature to C. The first and the second ones are split into two levels: "Low" and "High"; the third one is organised in three levels: "Low", "Medium" and "High".
Numerical values corresponding to those labels are: 30 and 60 min for reaction time (t); 4 and 8% for mass fraction of TCHP (w_{TCHP}); 150, 170 and 190°C for temperature (T) **(**Table 11).

Table 11 *Assignment of numerical values to the levels of reaction time, mass fraction of TCHP and temperature.*

Factor	Level		
	Low	**Medium**	**High**
***t* / min**	30	-	60
w_{TCHP} / %	4	-	8
***T* / °C**	150	170	190

Reaction time (t), mass fraction of TCHP (w_{TCHP}), temperature (T), interaction between t and w_{TCHP} and between w_{TCHP} and T are the main effects; interaction between t and T is confused with T, as one can deduce from Table 9.

The response variables are calculated applying the definitions given by Schmidt (1998). If one mole of TCHP is assumed to give one mole of 16-hexadecanolide (Figure 5) and density is considered to be constant, then:

$$\alpha = \frac{C_{TCHP_0} - C_{TCHP}}{C_{TCHP_0}}, \qquad \text{Eq. 25}$$

$$S = \frac{C_{16-Hex}}{C_{TCHP_0} - C_{TCHP}} \qquad \text{Eq. 26}$$

and

$$Y = \alpha \cdot S, \qquad \text{Eq. 27}$$

where X is conversion, S is selectivity, Y is yield. C_{TCHP_0} is the initial concentration of TCHP; C_{TCHP} and $C_{16\text{-}Hex}$ are the concentration of TCHP and 16-hexadecanolide respectively, calculated at the end of the reaction time. All the concentrations are evaluated via HPLC following the procedure described in §5.3.2 and expressed in mol·ml^{-1}. Eight experiments are carried out according to Table 16 and their results are shown in Table 12.

Table 12 *Conversion, Selectivity and Yield*

Exp.	Factors			Response variables		
	***t*/min**	**w_{TCHTP}/%**	***T*/°C**	***α***	***S***	***Y***
1	30	4	150	0.20	0.19	0.04
2	30	4	190	1.00	0.17	0.17
3	30	8	190	1.00	0.18	0.18
4	30	8	150	0.22	0.28	0.06
5	60	4	170	1.00	0.16	0.16
6	60	4	170	1.00	0.14	0.14
7	60	8	170	1.00	0.17	0.17
8	60	8	170	1.00	0.17	0.17

ANOVA is applied to those results to obtain the following conclusions.

Conversion

Pareto's chart of conversion is reported in Figure 16. α is mostly affected by temperature and time (blue columns), explaining together almost the total variability.

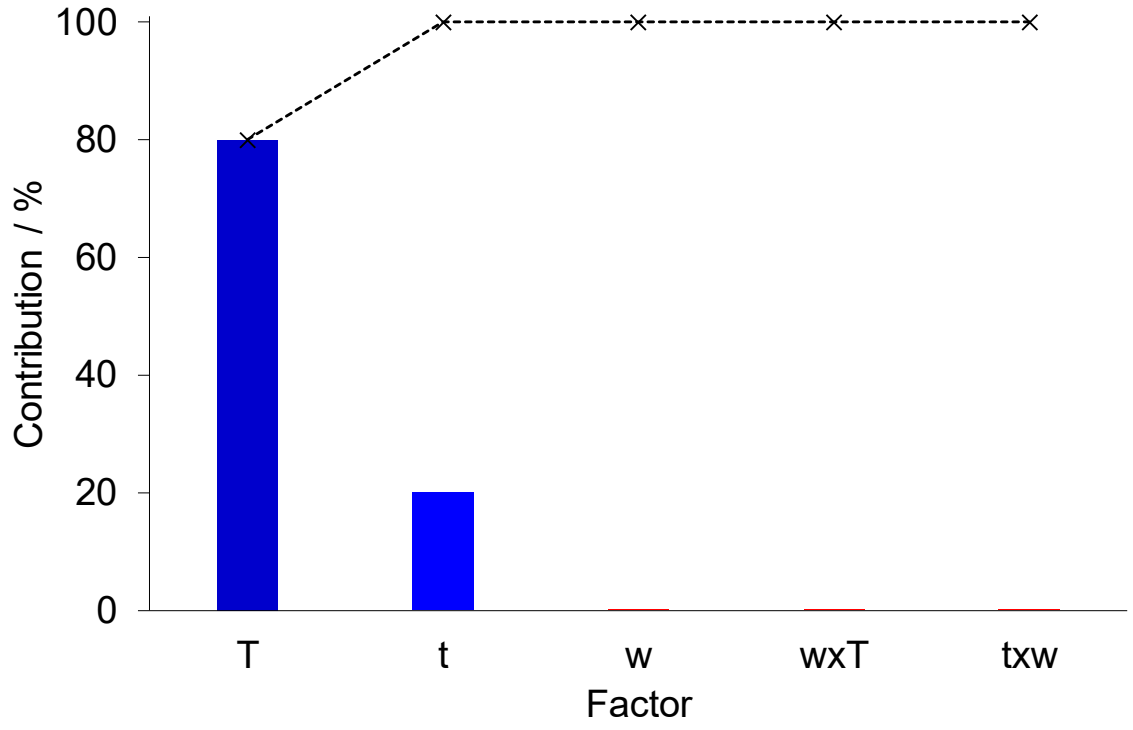

Figure 16. *Pareto's diagram for conversion (α) response variable. x-axis: Factors; y-axis: single factor's percentage contribution to explained variability on bars, cumulative contribution on dashed line. Blue bars: significant factors; red bar: non-significant factors.*

Temperature itself reaches a percent explained variability practically equal to 80 %, whereas reaction time provides the remaining 20 %.

Mass fraction of TCHP and interactions included in main effects affects for less than 10^{-2}, so they can be accounted for the experimental error. It is reasonable to conclude that conversion is not affected by the initial amount of reagent since it is normalised by it.

The conversion dependence on the relevant factor is further investigated studying its tendency between their levels. Figure 17 shows the effect of reaction time and temperature moving through their levels.

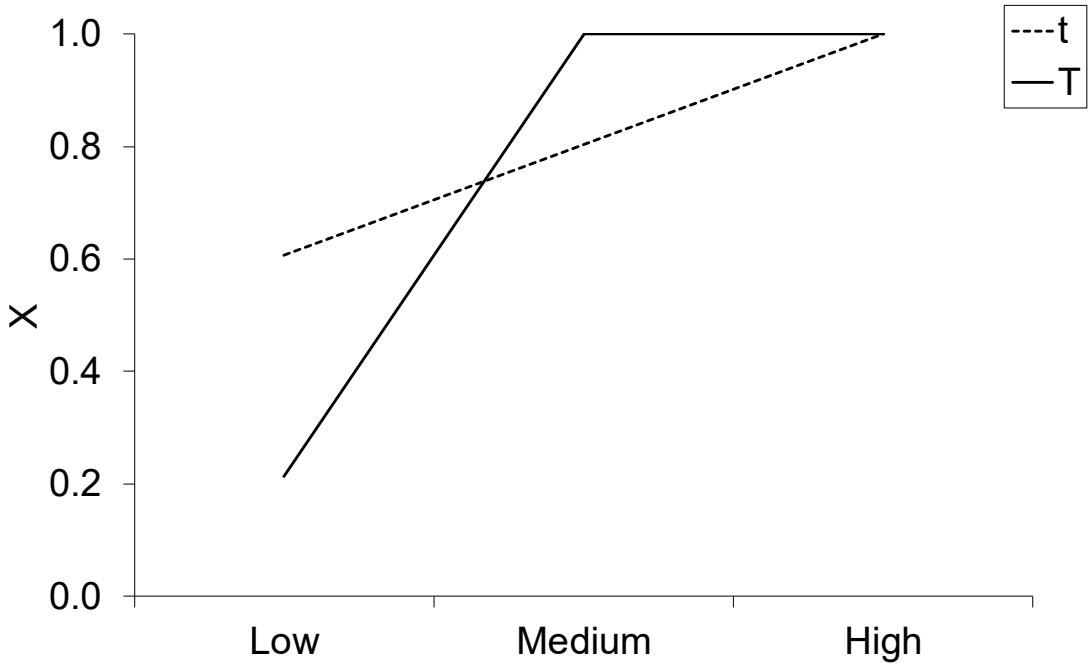

Figure 17. *Effect of statistically significant factors on conversion (X). Dashed line: reaction time (t); full line: temperature (T). Low, Medium and High are levels of the factors.*

It is observed that increasing temperature from 150 and 170°C makes the conversion increasing by almost five times. Moving from 170°C to 190°C does not provide any improvement of conversion. An increase of conversion due to an increase of temperature is what it is expected by a thermal activated reaction. When reaction time is changed from 30 to 60 min, α increases significantly because the decomposition of TCHP needs longer reaction times to occur.

A variation of *T* and *t* in the same direction generate an effect on conversion in the same direction, but temperature itself explain 80 % of variability. *T* x *t* interaction is confused in *T* one. Indeed, *T* x *t* effect cannot be more than the one of reaction time itself, which is four times lower than the *T* one. So, *T* x *t* interaction can be neglected with respect to the effect of *T*.

Total conversion is observed for Medium and High level of temperature and for High level of time.

Selectivity

Pareto's analysis of variance applied to selectivity gives the results shown in Figure 18.

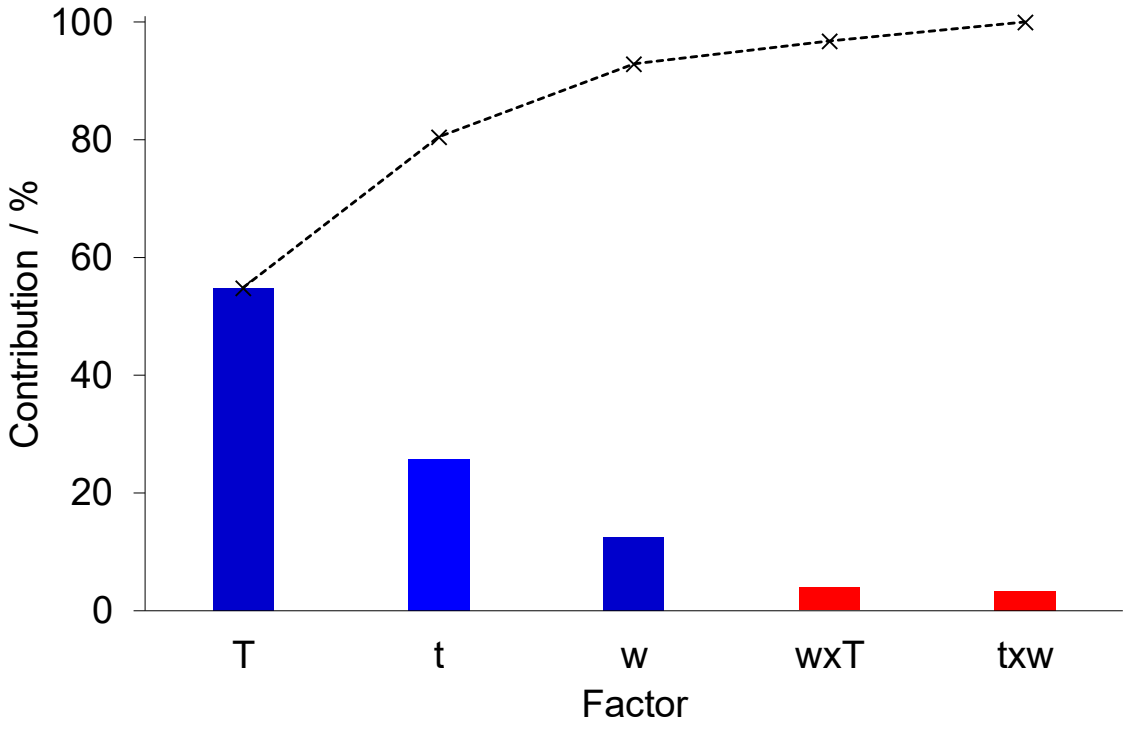

Figure 18. *Pareto's diagram for selectivity (S) response variable. x-axis: Factors; y-axis: single factor's percentage contribution to explained variability on bars, cumulative contribution on dashed line. Blue bars: significant factors; red bar: non-significant factors.*

Selectivity is significantly affected by temperature, reaction time and concentration, explaining about 55 %, 26 % and 12 % of the variability respectively. Other main effects can be treated as experimental error because an accumulated explained variability greater than 95 % is calculated. The influence of the relevant main effect's level on *selec*tivity is shown in Figure ***19***.

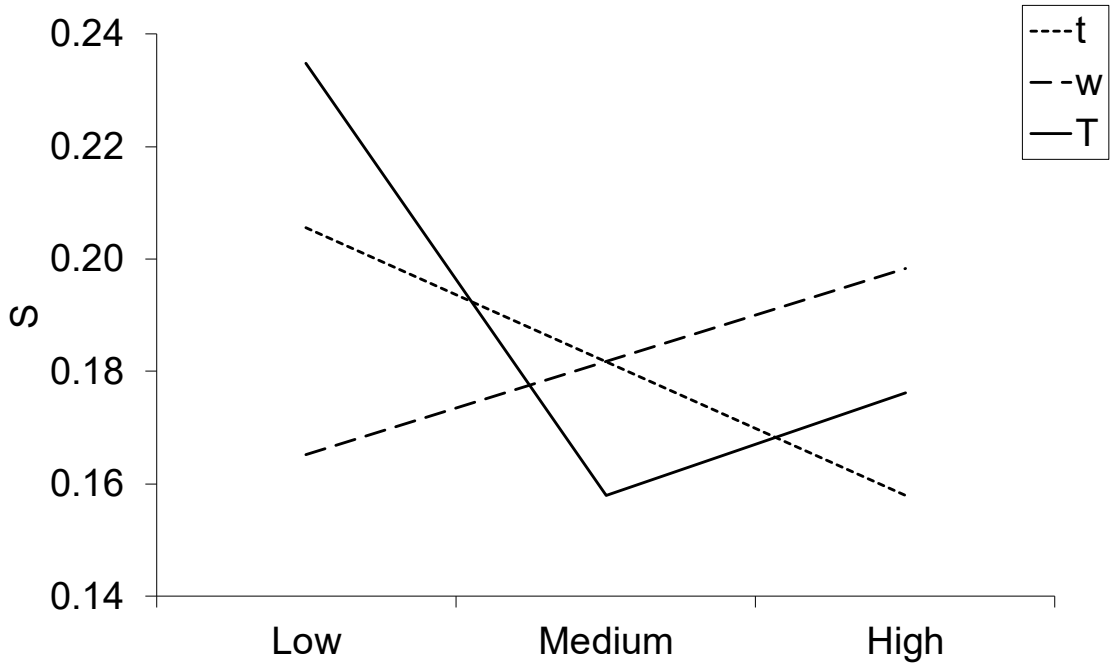

Figure 19. *Effect of statistically significant factors on selectivity (S). Dashed line: reaction time (t); dotted line: initial mass fraction of TCHP (w_{TCHP}); full line: temperature (T). Low, Medium and High are levels of the factors*

Selectivity is higher (around 0.24) when temperature is set on its low level (150 °C) and tends to decrease changing for its medium level (170 °C), slightly increasing again when *T* is 190 °C. Reaction time and initial concentration show an opposite effect. Switching from 30 min to 60 min induces a decrease of selectivity, whereas it grows moving from an initial mass fraction of TCHP of 4 % to 8 %. Just looking at those results it seems that 16-hexadecanolide formation is enhanced when TCHP is less reacted, *i.e.* when temperature and time are in their lower level. From its point of view, 16-hexadecanolide formation should be favoured at low conversions and with a higher initial mass fraction of TCHP.

Yield

Conversion and selectivity are two independent responses that can be joint in one dependent variable, the yield. It is calculated using Eq. 3. Pareto's analysis of variance applied to *Y* provides a way to identify the conditions to carry out the thermal decomposition of TCHP with respect to a unique response variable. Results are reported in Figure 20.

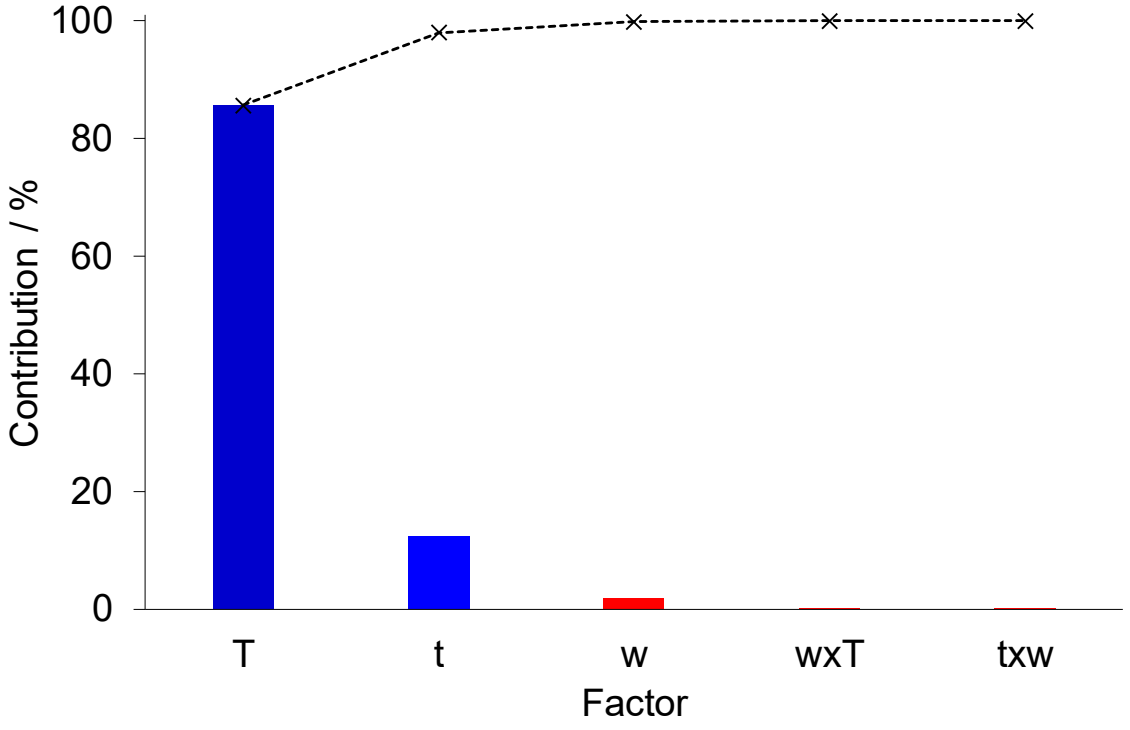

Figure 20. *Pareto's diagram for yield (Y) response variable. x-axis: Factors; y-axis: single factor's percentage contribution to explained variability on bars, cumulative contribution on dashed line. Blue bars: significant factors; red bar: non-significant factors.*

Temperature and time explain 86 % and 12 % of the variability of yield respectively, giving a cumulative contribution greater than 95 %.

Mass fraction of TCHP and all the interactions ranked among main effects are negligible due to their statistical irrelevance and considered as experimental error. Figure 21 describes the behaviour of yield when temperature and time are changed among their levels.

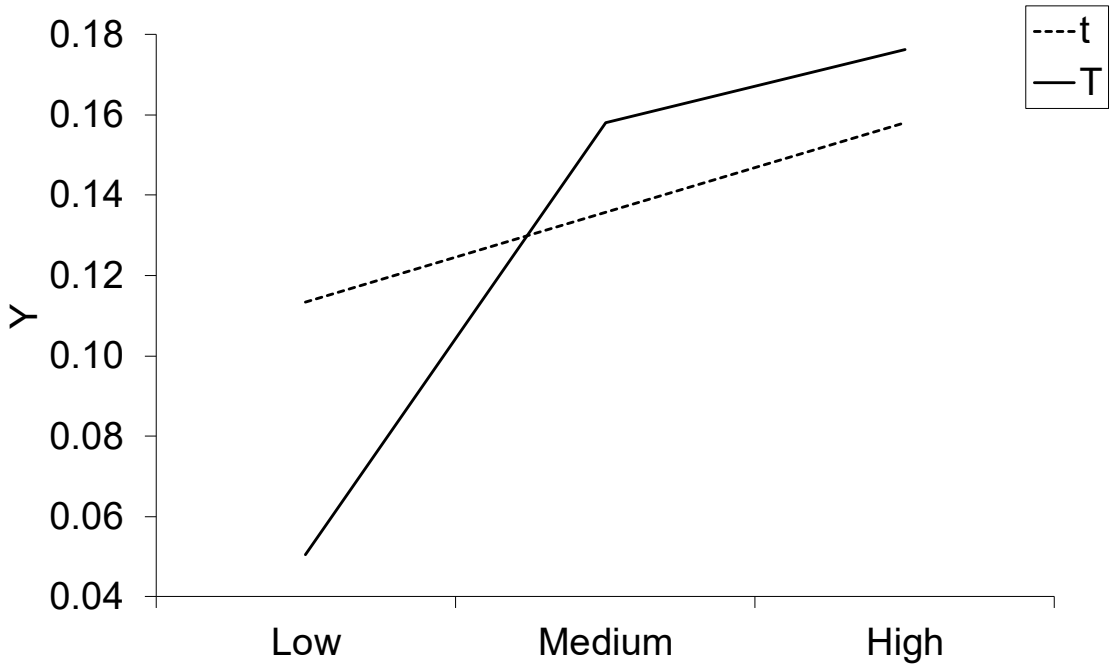

Figure 21. *Effect of statistically significant factors on yield (Y). Dashed line: reaction time (t); full line: temperature (T). Low, Medium and High are levels of the factors*

Making temperature growing from 150 °C to 170 °C leads yield to be increased by almost four times, up to a value of 0.16. A further addition of twenty degrees as not the same influence, bringing an improvement of 2%.

An increase of time has a positive effect on yield. The tendencies on conversion of Figure 21 are mostly affected by *T* and *t*. In particular, yield of reaction is greatly undermined if conversion is not complete (150 °C and 30 min). In other words, TCHP has to react as much as possible if obtaining high yields is desired.

Using a more concentrated reactant mixture has a positive effect on selectivity. However, here it is demonstrated that it does not have any drawback on *Y*. Other authors' works, entirely focused on optimizing the selectivity to 16-hexadecanolide, provide values between 0.23 and 0.19 (de Armas, 2015). Indeed, a quantitative improvement cannot be reached in this direction just changing the factors considered here.

Regarding the eventuality to carry out the reaction with higher concentration of TCHP, it must be taken into account that its extreme exothermicity determines a 10 % w/w limit for industrial applications.

For all those reasons, the thermal decomposition of TCHP will be performed at 170 °C with an initial mass fraction of reagent of 4 %, for a reaction time long enough to get complete conversion.

As conclusive remark, it has to be considered that the reaction is performed in 5 ml vial without any mixing system, but isothermal condition can be assumed considering the volume of the furnace much greater than the reacting one.
However, it is emphasised that the purpose of this work is not optimising the thermal decomposition of TCHP inside a true batch reactor, but performing it in a flow one. In this sense, those experiments are useful in clarifying which conditions promote the conversion of TCHP and the formation of 16-hexadecanolide and which ones penalise them.

Chapter 4

Flow reactors

In this Chapter is described how the decomposition of tricyclohexylidene triperoxide is carried out in continuous using flow chemistry techniques. Two layouts are investigated and compared: a tubular reactor and a tube-in-tube reactor.
Finally, it is demonstrated that the latter is more reliable and suitable for a safer industrial production of 16-hexadecanolide.

4.1 Modelling continuous reactors for TCHP decomposition

16-hexadecanolide can be obtained from the thermal decomposition of TCHP, according to the reaction reported in Figure 5. The conditions at which carry out the reaction were identified in Chapter 3 and are reported here for clarity.

Table 13. *Conditions to perform the thermal decomposition of TCHP.*

Reagent	TCHP
Solvent	*n*-dodecane
w_{TCHP} / %	4
T / °C	170

The continuous operations are performed using either a tubular rector or a tube-in-tube one. Both have tubular shape with small diameter section.
The easiest model to predict the conversion profile of such a system is the plug flow reactor (PFR) model. The basic equation to be solved is its material balance (Schmidt, 2002):

$$\bar{u}\frac{\mathrm{d}\,c_i}{\mathrm{d}\,z} = \upsilon_i r\,. \qquad \text{Eq. 28}$$

where c_i is the concentration of the species i, z is the axial coordinate of the cylinder, υ_i is the stoichiometric coefficient of species i and r is the reaction rate in moles·time^{-1} and $\bar{u}$ is the mean fluid velocity inside the tube, defined as:

$$\bar{u} = \frac{V}{\dot{V}} \qquad \text{Eq. 29}$$

V is the reactor volume and $\dot{V}$ is the volumetric flowrate.
Eq. 28 can be rearranged in terms of conversion (α) introducing the kinetic law mentioned in Eq. 23:

$$\frac{\mathrm{d}\,\alpha}{\mathrm{d}\,\tau} = A \cdot e^{-E_a/(R \cdot T)} \cdot \left[\gamma \cdot (1-\alpha) + \alpha^m \cdot (1-\alpha)^n\right], \qquad \text{Eq. 30}$$

where τ is the residence time,

$$\tau = \frac{z}{\overline{u}} \qquad \text{Eq. 31}$$

and all the kinetic parameters have the numerical values reported in Table 3.
That equation is based on the following assumptions:

1. Plug flow,
2. Steady state
3. Constant density
4. Constant tube diameter
5. Single reaction

Hypothesis 1 is usually satisfied when fluid dynamic regime is turbulent. However, flow chemistry reactors often show laminar flow. In that conditions, assuming plug flow is not correct anymore. For this reason, a more suitable reactor model has to be applied.
In laminar regime, velocity distribution is not flat. Radial dependence has to be introduced, as it shown in Figure 22.

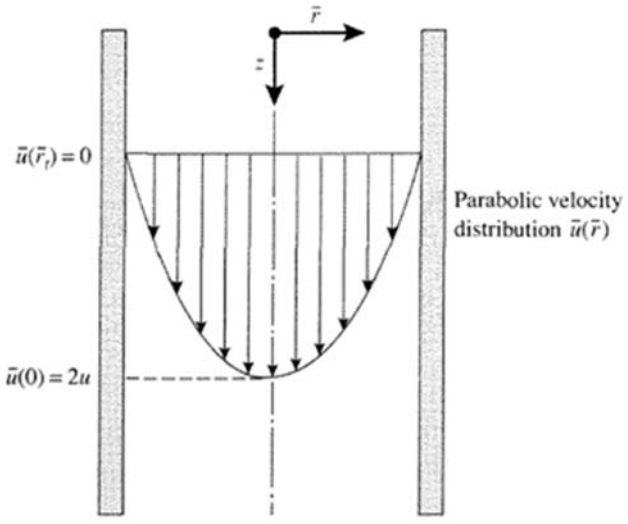

Figure 22. *Parabolic velocity distribution in laminar flow reactor. z is the axial coordinate; r s the radial coordinate; u($\overline{r}$) is the velocity distribution.*

The following equation describes the radial profile of velocity:

$$u(\bar{r}) = 2 \cdot \bar{u} \cdot \left[1 - \left(\frac{\bar{r}}{r_R} \right)^2 \right]. \qquad \text{Eq. 32}$$

$\bar{r}$ is the radial coordinate, $\bar{u}$ is defined in Eq. 29, and r_R is the internal radius of the reactor. Assuming negligible mass diffusion (in both axial and radial dimensions), mass balance for LFR is the same reported in Eq. 28, but the radial dependence of velocity is introduced:

$$u(\bar{r}) \cdot \frac{\mathrm{d}\, c_i}{\mathrm{d}\, z} = -r \qquad \text{Eq. 33}$$

$\upsilon_i = -1$ is the stoichiometric coefficient of TCHP according to the reaction of Figure 5.
r is expressed using the kinetic law of Eq. 23, rearranged in terms of TCHP concentration:

$$r = -c_0 \cdot \frac{\mathrm{d}\, \alpha}{\mathrm{d}\, t} = -c_0 \cdot A \cdot e^{-E_a/(R \cdot T)} \cdot \left[\gamma \cdot \left(\frac{c}{c_0} \right) + \left(1 - \frac{c}{c_0} \right)^m \cdot \left(\frac{c}{c_0} \right)^n \right] \qquad \text{Eq. 34}$$

Since $u(\bar{r})$ does not depend on the axial coordinate z, Eq. 34 can be integrated between 0 and a generic position on axial coordinate, z:

$$\int_{c_0}^{c} \frac{\mathrm{d}\, c}{r} = u(\bar{r}) \cdot \int_0^z \mathrm{d}\, z \Rightarrow c(\bar{r}, z) = \mathrm{f}(u(\bar{r}), z) \qquad \text{Eq. 35}$$

The mean concentration over a section is obtained integrating on the radial dimension as follows:

$$\bar{c} = \frac{\int_0^{r_R} c(\bar{r}, z) \cdot u(\bar{r}) \cdot 2\pi \cdot \bar{r} \cdot \mathrm{d}\, \bar{r}}{\int_0^{r_R} u(\bar{r}) \cdot 2\pi \cdot \bar{r} \cdot \mathrm{d}\, \bar{r}} \qquad \text{Eq. 36}$$

Eq. 32, 34 and 36 are implemented in a MATLAB® code to calculate the conversion profile. In Figure 23 the result of the simulation is reported using the same kinetic law, at T = 170°C.

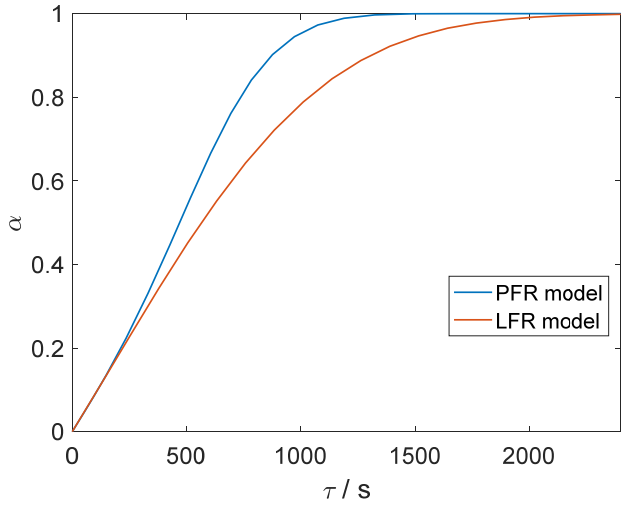

Figure 23. *Simulation of PFR model (blue line) and LFR model (red line). Kinetic law from Eq. 23 calculated at T = 170°C.*

The two models provide similar conversion profiles for low residence time (less than 250 s, but LFR model takes roughly double the time to get complete conversion.

4.2 Tubular reactor

Tubular reactor is build following the procedure described in §5.6. Figure 24 provides a schematic representation of the system.

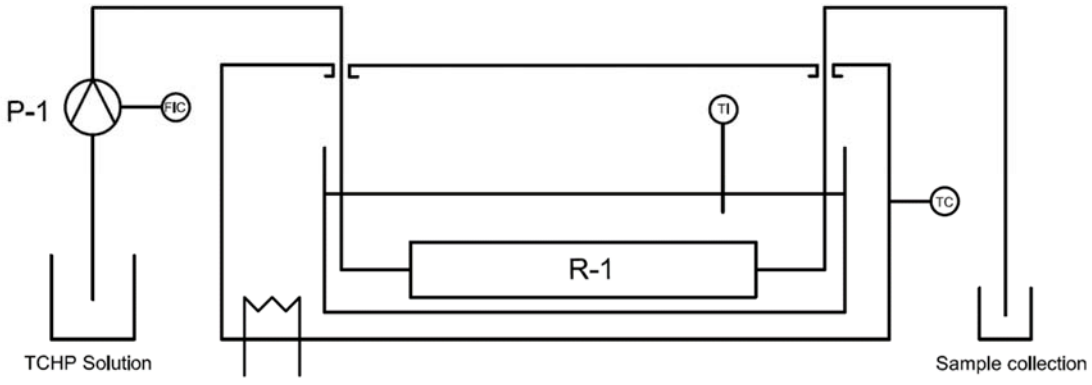

Figure 24. *Schematic representation of the tubular reactor layout. P-1: piston pump; FIC: flowrate controller of P-1; R-1: reactor; TI: temperature sensor inside the silicon bath; TC: oven's temperature control system.*

Reactor length is fixed, so experiments are carried out changing the flowrate of the pump. In that way, several residence times can be explored and then conversion profile experimentally determined.

Reaction is supposed to be performed isothermally and the reactor is modeled on this assumption. However, actual temperature control is not precise enough to apply that hypothesis to the experimental set-up. According to the precision of the instrumentation, a temperature interval between 173 and 176°C is considered the proper one to interpret experimental data.

Silicon bath is mandatory to provide fast heating also at high flowrates. Furnace's air under natural convection was observed to be unsuitable as heating medium. This is due to the combination of its low heat capacity and high resistance to thermal diffusion of Teflon®.

Injection flowrate of TCHP solution determines the reactor's fluid dynamic regime. Reynolds Number can be calculated from data reported in Table 17 (§5.6). Fluid properties are considered the ones of *n*-dodecane.

Reynolds Number is between 0.6 and 122.9 so the fluid dynamics regime is clearly laminar. Since the reaction is monomolecular, internal diffusion or mixing are not an issue. In other words, the system can be considered in kinetic control, or mass transfer can be directly neglected. Laminar flow does not affect the reaction in that sense.

Any resistance to heat diffusion inside the tube can be overcome estimating a "heating length" to achieve the desired temperature. 8 s are estimated for the actual experimental set up. Very small reactor diameter also allows to neglect any effect of a temperature profile.

What is really affected by laminar flow is the residence time distribution. Comparing two reactors of the same length, the mean concentration profile is lower in the LFR one, as it is demonstrated in Figure 23.

Gas generation during TCHP decomposition is something that could even affect the fluid dynamics of the reactor. Reagent itself is dissolved in liquid phase, but the system becomes biphasic when CO_2 is generated.

In Figure 25 experimental points of conversion (α) are reported. In the same plot, PFR and LFR models are simulated at the average temperature of 174.5°C.

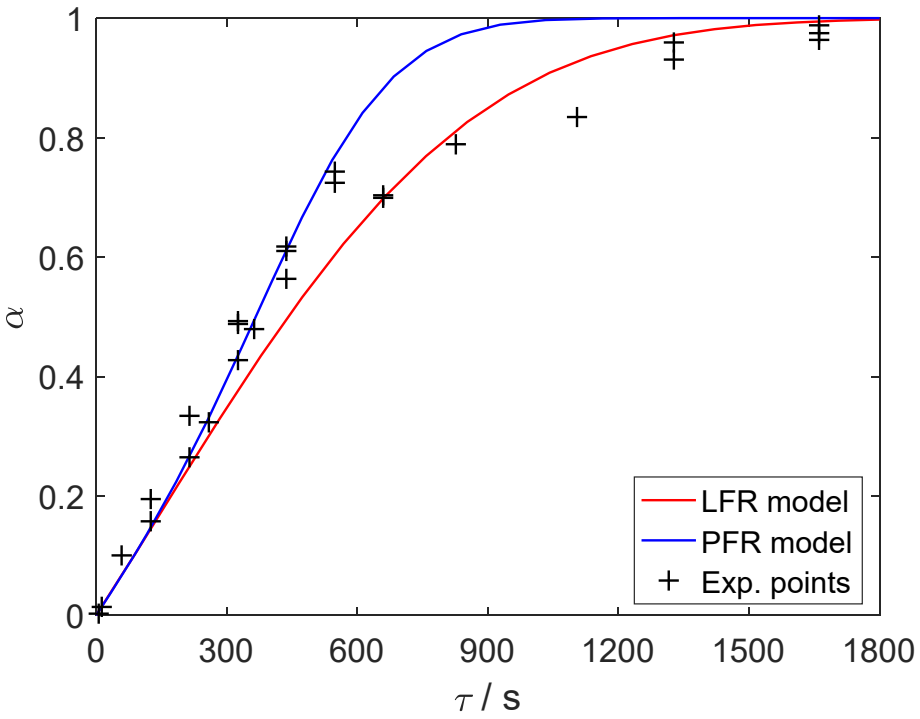

Figure 25. *Tubular reactor's conversion (α) profile vs residence time (τ). Crosses: experimental points; lines: PFR model (blue) and LFR model (red) simulated curves. T = 174.5°C.*

Complete conversion is achieved in about 1650 s (27.5 min).

Experimental points follow two different tendencies. PFR model accurately reproduces empirical data for values of τ lower than 600 s, corresponding to conversions between 0 and 75 %. LFR is more adequate for higher values of conversion and residence time. One single model cannot be used to predict the complete profile.

Gas formation could lead to the expansion of the reacting volume. An increase of the liquid velocity, pushed by CO_2, would end in a decrease of the time spent inside the reactor. A conversion lower than the predicted would be observed.

Each point of Figure 25 is obtained operating the reactor in laminar flow: LFR model should fit also low conversion points. Moreover, simulated curves are different enough to distinguish the different behaviours.

A possible interpretation of this behaviour can be that CO_2 generated by the decomposition has the effect of breaking the regularity of laminar layers, introducing kind of turbulent flow. This effect should be enhanced at low conversions, where bubbles are tiny and do not coalesce. In this particular condition they tend to produce a segmentation of liquid phase continuity.

Transition to ideal laminar flow model occurs when the amount of CO_2 generated is such that bubbles join together giving rise to gas pockets well segregated from liquid phase. The continuity of liquid phase is not so perturbed anymore. High conversions need low fluid

velocity to be reached, since the length of reactor is fixed. The combination of low velocities and the ever greater gas generation could lead to a situation in which large pockets of gas are spaced by liquid sections flowing in laminar regime.
This hypothetical explanation for the transition between one and the other behaviour is supported by empirical evidences. When experiments were performed, the gas-phase system inside the reactor showed the abovementioned fragmentation (for low conversion trials) and segregation, when higher conversions had to be reached.
Extracting gas while it is generated is a way to better understand what is actually occurring. This is what will be done in the next paragraph.
Before this, selectivity and yield in 16-hexadecanolide are calculated and reported in the following figures.

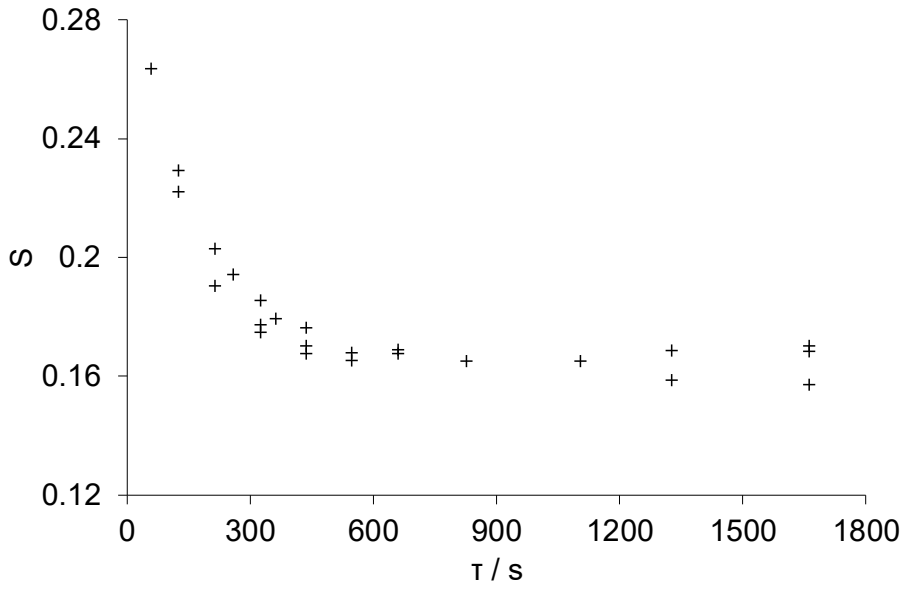

Figure 26. *Selectivity (S) in 16-hexadecanolide calculated at different conversions and plotted in function of residence time τ, for tubular reactor.*

Selectivity profile in function of residence time shows a decreasing shape. Its maximum theoretical value is 1, since the only reaction producing 16-hexadecanolide is the one reported in Figure 5.
Starting from its highest value (0.26) at about 10% of conversion, it decreases and then settles into 0.16 after 500 s of reaction or when about 50 % of the initial TCHP has reacted.
Just looking at that plot, it would be concluded that working at low conversions could be an option, in agreement on what was concluded in §3.2.2.
However, arranging conversion and selectivity with yield, leads to another outcome.

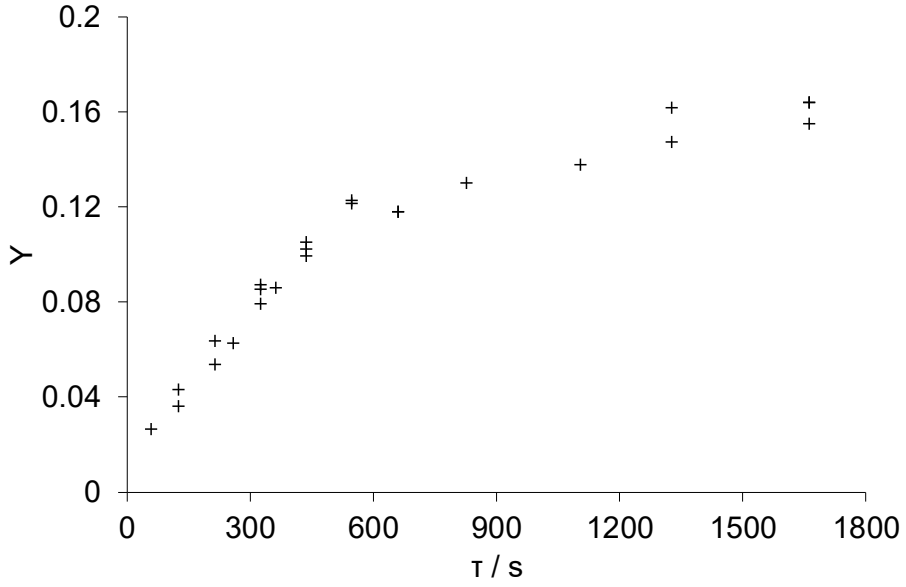

Figure 27. *Yield (Y) in 16-hexadecanolide calculated at different conversions and plotted in function of residence time τ, for tubular reactor.*

Yield increases increasing residence time, following an opposite tendency to selectivity. That means that even if selectivity decreases while TCHP is reacting, it settles into a value high enough to justify pushing the reaction to its maximum conversion.
After 27.5 min, yield is equal to about 0.16, $\alpha = 0.98$ and *S* just above 0.16.

4.3 Tube-in-tube reactor

CO_2 extraction is achievable performing TCHP decomposition in tube, made of gas permeable membrane, Teflon® AF2400. Thermal stability of this material is ensured until 260°C; it does not show any weight loss after 4 hours at that temperature. Chemical compounds involved in TCHP decomposition are not affecting the chemical resistance of Teflon® AF2400 (Resnick and Buck, 1997).
The tube-in-tube reactor is built following the procedure described in §5.7. A schematic representation of the system is reported in Figure 28.
Reaction conditions are the same as the ones adopted in tubular reactor experiments (Table 13).

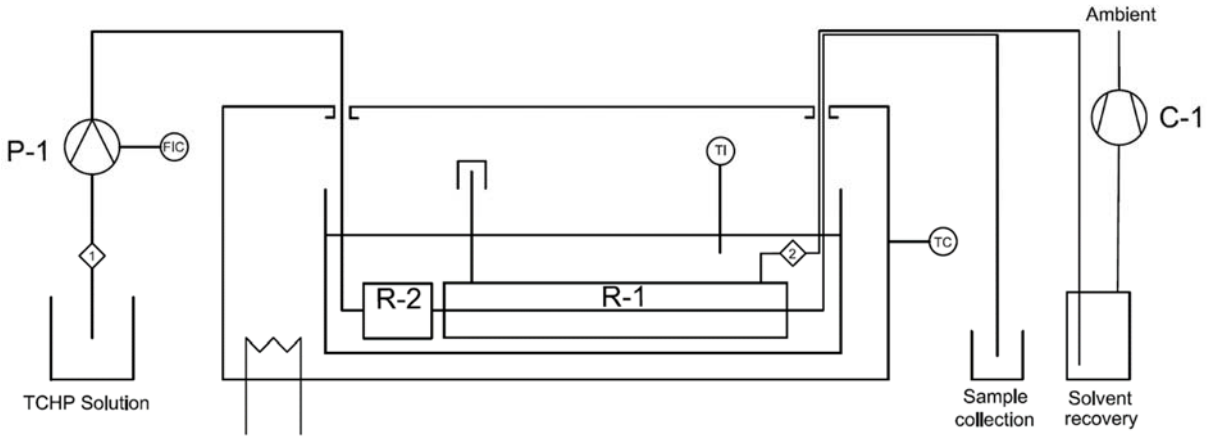

Figure 28. *Schematic representation of the tube-in-tube reactor layout. P-1: syringe pump; FIC: flowrate controller of P-1; R-1: tube-in-tube reactor; R-2: reactor heating section; TI: temperature indicator inside the silicon bath; TC: oven's temperature control system; C-1: vacuum pump. Stream 1: liquid TCHP's solution stream; Stream 2: extracted gas stream.*

TCHP dissolved in *n*-dodecane at ambient temperature (Stream 1) is made flowing using a syringe pump (P-1) inside the tube-in-tube reactor (R-1). It is submerged in silicon bath, which in turn is placed inside an oven.

Crude reaction mixture exits the oven and is collect and analyzed via HPLC (§5.3.2).

The operating principle is to set under vacuum the annular space between two tubes and extracting CO_2 (Stream 2), that permeates through the membrane.

CO_2 is the main gaseous product of TCHP decomposition. However, the combination of high temperatures ($\geq 170°C$) and vacuum can induce the evaporation of other compounds. When they exit the oven and reach ambient temperature, condensation occurs. A solvent recovery flask is set on gas outlet, to avoid having droplets of liquid inside the vacuum pump (C-1).

The content of the solvent recovery flask was qualitatively analysed via HPLC at the end of a set of experiments. Cyclohexanone and *n*-dodecane are its main components.

Many trials were done to understand how to heat reagent's solution to reaction temperature and to maintain it during reaction progress, *i.e.* inside the membrane reactor.

A first attempt is made to exploit the insulation generated by vacuum. Reactor's active length is left outside the oven and a small portion of standard Teflon® tube served as heating section.

A second attempt consists in submerge both the heating section and the actual tube-in-tube inside the silicon, leaving the connections at ambient temperature.

In both cases, even if vacuum is an insulant, heat losses are too much to keep the suitable temperature for TCHP decomposition.

Layout of Figure 28 requires high temperature resistant connections, that allowed submerging the whole system inside the silicon bath. A short portion of standard Teflon® tube (R-2) comes first the tube-in-tube section to heat up TCHP solution.
Once the layout is set up, a set of experiments is performed following the procedure described in §5.7.
It is considered a temperature interval between 174 and 177°C. Laminar flow is verified again, having calculated a Reynolds number of 0.7 and 3.8 for the lowest and highest flowrate, respectively.
In Figure 29 experimental conversions (α) are plotted in function of residence time (τ). In the same figure, PFR and LFR models are simulated at the average temperature of 174.5°C.

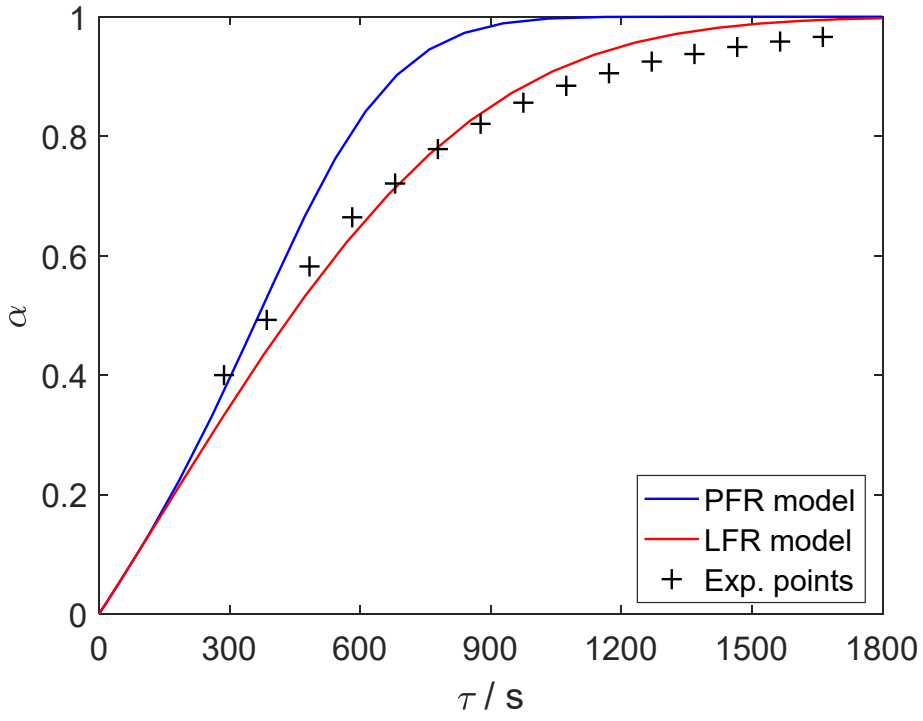

Figure 29. *Tube-in-tube reactor's conversion (α) profile vs residence time (τ). Crosses: experimental points; lines: PFR model (blue) and LFR model (red) simulated curves. T = 174.5°C.*

Some qualitative observations can be done.
Firstly, the experimental noise of the data is significantly lower than using the tubular system. Unlike the tubular reactor, conversion always increases increasing residence time.
Secondly, 97.5 % of TCHP reacts with a residence time of 27.5 min (1650 s): the same happens using tubular rector.

Thirdly, LFR model adequately predicts experimental points, for the range in which the two models are different enough. No transition region is observed between 5 (300 s) and 10 min (600 s) and PFR model never fits experimental conversions.
Given that, removing CO_2 produces an improvement in the prediction of conversion profile. Flow regime is laminar and LFR model correctly reproduces experimental data
Gas formation would lead to unpredictable behavior of the system. Then, the advantage of using a tube-in-tube reactor is that the fluid dynamics is not affected anymore.
Two evidences confirm that the supposed change of density due to CO_2 formation does not affect significantly the prediction of residence time. The first: LFR model assumes of constant density and it adequately predicts experimental data. The second: complete conversion is reached around the same residence time in both tubular and tube-in-tube reactors.
Even if LFR model provides an effectively prevision of experimental conversions, an empirical model based on polynomial regression can be introduced to practically facilitate a quantitative comparison between models.
Since experimental points follow a coherent and regular tendency, a second order polynomial is sufficient. It is remarked that it has no physical meaning, but it is just a way to reproduce empirical data with high accuracy inside the experimental domain:

$$\alpha = a_2 \cdot \tau^2 + a_1 \cdot \tau + a_0, \qquad \text{Eq. 37}$$

where $a_2 = -3.829 \cdot 10^{-7}$, $a_1 = 1.124 \cdot 10^{-3}$, $a_0 = 0.1.296 \cdot 10^{-1}$.
A first quantitative indication way to compare different models is calculating the mean squared error (e), using the following equation:

$$e = \frac{\sum_{1}^{n} \left(\alpha_{th}(\tau_n) - \alpha_{\exp}(\tau_n)\right)^2}{n} \qquad \text{Eq. 38}$$

where n is the number of experimental points, α_{th} and α_{exp} are respectively the theoretical and the experimental values of conversion taken at the n^{th} experimental residence time τ_n.
Eq. 38 is used to calculate the error of the model-estimated conversion with respect to the experimental one, for each reactor layout (tubular or Tube-in-Tube). Error values are normalised by the minimum one, *i.e.* the one obtained by the polynomial. The greater the difference from one, the greater the inaccuracy of the model.

Table 14 *normalised mean squared error between experimental and PFR, LFR, combination of PFR and LFR and polynomial model predicted conversion for tubular and tube-in-tube reactors.*

	PFR model	LFR model	PFR and LFR models	2nd order polynomial
Tubular	45.4	36.9	9.2	-
Tube-in-Tube	83.1	10	-	1

As it was qualitatively observed before, tubular reactor is not totally predictable by one single model. Using a combination of both PFR and LFR model gives a result that is comparable to the one obtained using just LFR model for the tube-in-tube reactor.

The polynomial of Eq. 41 is reported in Figure 27 (green line). Tube in tube reactor's conversion is on the *x*-axis, whereas the residence time on the right-hand *y*-axis.

It is then used to calculate the conversion at the experimental residence time of tubular reactor. Experimental conversion of tubular reactor (left-hand *y*-axis) and the one predicted by the polynomial (*x*-axis) are plotted giving rise to the crosses of Figure 27. If tubular reactor and tube-in-tube reactor provided the same results, all the crosses would be on the black line.

Linear regression of those points gives the red line of Figure 27. It has no significant difference from the black one. That means that, despite the greater noise of the tubular, both reactors follow the same model, the polynomial one. In principle, this conclusion is strictly related to the polynomial model. Since tubular reactor's experimental points are predicted with a good accuracy using LFR model, the conclusion could also be extended to that one.

Moreover, most of the points are below the black line, meaning that the conversion in the tubular reactor is lower than the one expected using the empirical model obtained from the tube-in-tube reactor data. The main deviation from that behaviour is confined between about 45 % and 70 % conversion (*x*-axis) corresponding to a residence time between 300 and 600 s. this is exactly the region where gas generation is thought to modify the fluid dynamics. Tube-in-tube reactor is then better in all the residence times, except the previous ones, where the behaviour of the tubular reactor is closer to the PFR one.

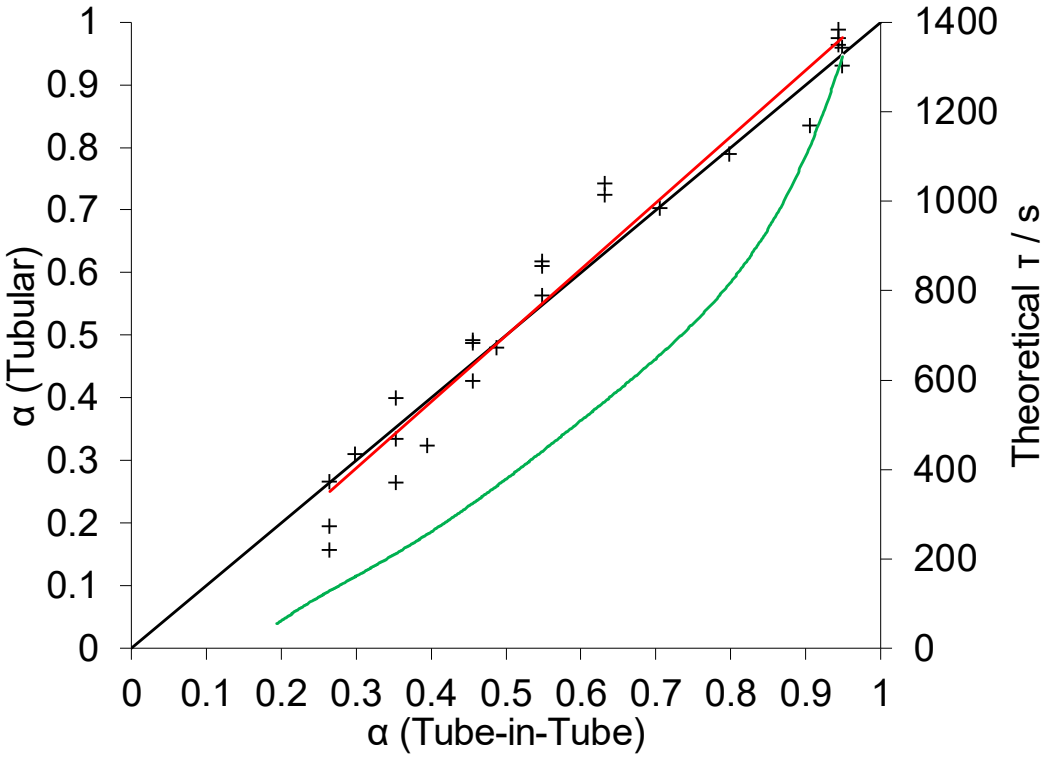

Figure 30. *Experimental (left-hand* y*-axis) and predicted (*x*-axis) conversion of tubular reactor (crosses) and their linear regression (red line). Polynomial fitting of tube-in-tube experimental points (green line): conversion (x axis) vs residence time (right hand y axis).*

To conclude the analysis of the tube-in-tube reactor, the plots of experimental selectivity and yield in 16-hexadecanolide are reported below.

Selectivity basically oscillates around 0.17 (Figure 31), a value comparable than the one obtained with tubular reactor. Since some *n*-dodecane is extracted, crude reaction mixture is a bit more concentrated. This occurrence could determine the above increase.

The overall trend is pretty similar to tubular reactor's one. Experiments at low residence times were not performed, but for $\tau \geq 300$ s the selectivity became constant.

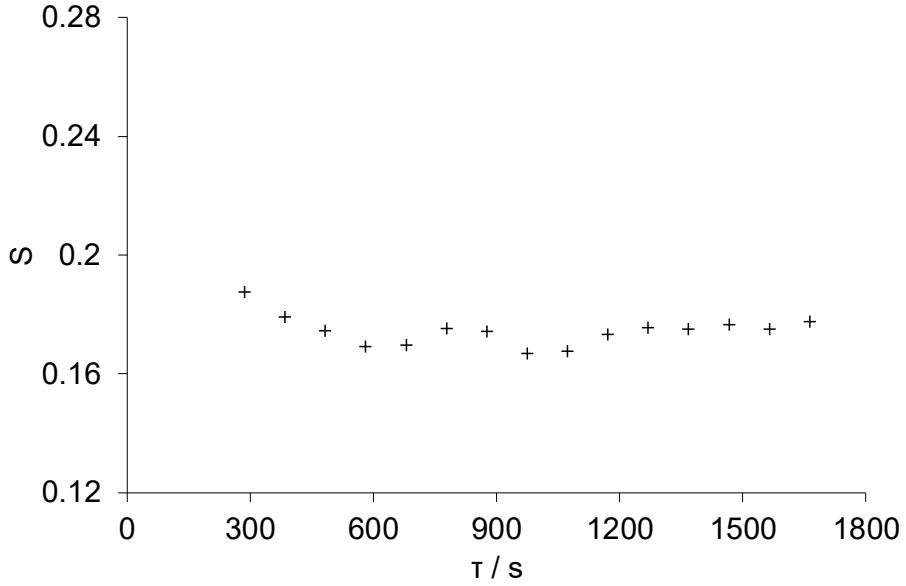

Figure 31. *Selectivity (S) in 16-hexadecanolide calculated at different conversions and plotted in function of residence time τ, for tube-in-tube reactor.*

Yield in 16-hexadecanolide increases increasing the residence time. Since selectivity can be considered constant, it means that the higher the conversion, the higher the yield. A final value of 0.17 is calculated, with $S = 0.18$ and $\alpha = 0.97$.

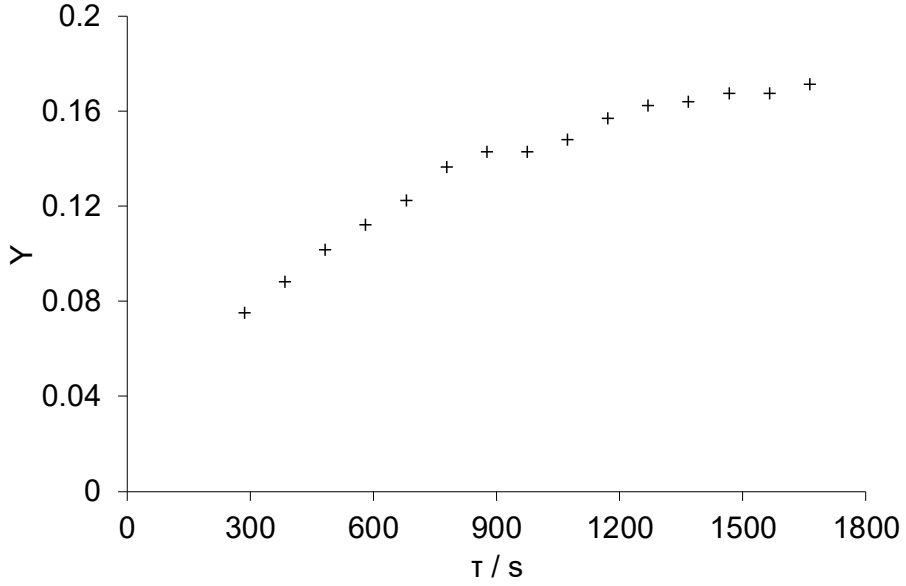

Figure 32. *Yield (Y) in 16-hexadecanolide calculated at different conversions and plotted in function of residence time τ, for tube-in-tube reactor.*

Since selectivity is not considerably changing during reaction progress, conversion has to be pushed to its maximum to obtain the maximum yield.

Chapter 5

Experimental part

In this Chapter it is reported all the information concerning the equipment and the materials involved in this work. Subsequently, the analytical methods are described in detail. In the last paragraphs, it is explained the build-up of flow reactors.

5.1 Equipment

Mettler Toledo DSC 821^e is used to obtain the differential scanning calorimetry records. Samples are weighted using a Mettler Toledo XS3DU microbalance. The records are evaluated by the S**TA**R v. 11 Software of Mettler Toledo.
All the chromatograms are obtained by an Agilent Technologies 1200 series HPLC, at the Laboratory of Chromatography of the IQS School of Engineering. It is a modular instrument composed by a Degasser (G1379B), a Pump (G1312B), a High Performance Autosampler (G1367C), a Thermostatted column compartment (G1316B), a Diode Array detector (DAD) (G1315C) and a Refractive Index detector (RID) (G1362A). Chromatograms are recorded and evaluated by OPEN LAB, version A.02.02 (1.3.4).
Teflon® AF2400 tube is provided by Biogeneral.

5.2 Solvents and reagents

Compounds involved in this work are listed below:

- Acetonitrile ≥ 99.9%, VWR Chemicals, CAS No. 75-05-8
- Cyclohexanone ≥ 99%, Fluka, CAS No. 108-94-1
- Dichloromethane 99%, PanReac, Cod. 141254
- 16-hexadecanolide 97%, Alfa Cesar, CAS No. 109-29-5
- Hydrogen peroxide 30% w/v, PanReac, CAS No. 7722-84-1
- Methanol 99.9%, PanReac, CAS No. 67-56-1
- *n*-dodecane 99%, Acros Organics, CAS No. 112-40-3
- Phosphotungstic acid hydrate, PanReac, CAS No. 235-087-6
- Tricyclohexylidene triperoxide 99%, provided by D. de Armas, Ph.D.
- Dicyclohexylidene Diperoxide 99%, provided by D. de Armas, Ph.D.

5.3 Analytical Methods

5.3.1 Differential scanning calorimetry

The equipment mentioned in §5.1 is used to perform the calorimetric analysis. Samples of solid TCHP and DCHP are prepared in a 70 µl standard crucible of aluminium (ME 00024123). The lid is previously pierced.
Experiments are performed with a heating rate of 10 $K \cdot min^{-1}$, in a temperature interval between 30 and 250°C in an inert atmosphere of nitrogen (constant flowrate of 50 $ml \cdot min^{-1}$).
The mass of each sample varies from 1.7 to 6 mg.

5.3.2 High performance liquid chromatography

Samples are analysed with HPLC technique using the system described in §5.1, equipped with a Nova-Pak® C18 column (4 µm, 3.9×150 mm).
The mobile phase is a mixture of acetonitrile and water (90:10 v/v) flowing at 1 $ml \cdot min^{-1}$, at 30°C. The DAD operates at the wavelength of 210 nm. Every analysis takes 15 min.
The following table summarizes the expected approximated retention times.

Table 15 *Approximated retention times*

Compound	t_{ret} / min
TCHP	6.6±0.1
DCHP	2.0±0.1
16-hexadecanolide	4.9±0.3

DAD detector calibration lines are calculated ones for all for TCHP and 16-hexadecanolide. For the first, the standard is considered to be the one synthetized following the procedure described in §5.4. For the second, the reference is the one listed in §5.2.
Four solutions at different concentrations of TCHP in *n*-dodecane are prepared and analysed. The peaks of the chromatograms are integrated and the relation between areas and concentration is found to be linear for $c \leq 0.04\ g \cdot ml^{-1}$.
Linear regression is applied to the points of the plot of concentration *vs* area of the peak, expressed in milli absorbance unit times seconds (mAU·s).
Linear regression coefficient is found to be equal to $5.862 \cdot 10^{-7}$, with an intercept of $-7.864 \cdot 10^{-4}$. Concentration (c) of TCHP is given in $g \cdot ml^{-1}$. The plot is reported below.

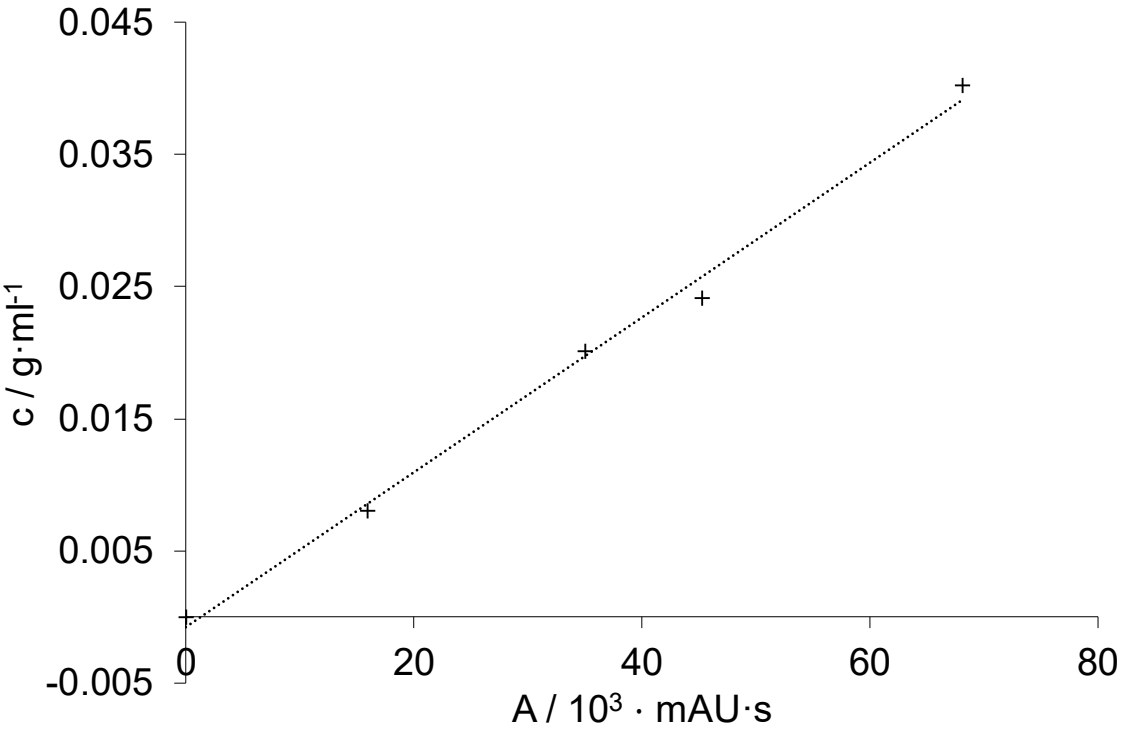

Figure 33. *DAD detector calibration points for TCHP and their linear regression. Slope: $5.862 \cdot 10^{-7}$; intercept: $-7.864 \cdot 10^{-4}$.*

Five solutions at different concentration of 16-hexadecanolide in acetonitrile are prepared and analysed, taking into account the 97% purity. The peaks of the chromatograms are manually integrated and the relation between areas and concentration is found to be linear for $c \leq 0.02$ g·ml^{-1}.

Linear regression is applied to the points of the plot of concentration *vs* area of the peak. The slope is found to be equal to $2.9 \cdot 10^{6}$ with an intercept equal to $2.5 \cdot 10^{-4}$. Concentration (c) of 16-hexadecanolide is given in g·ml^{-1}. The plot is reported below.

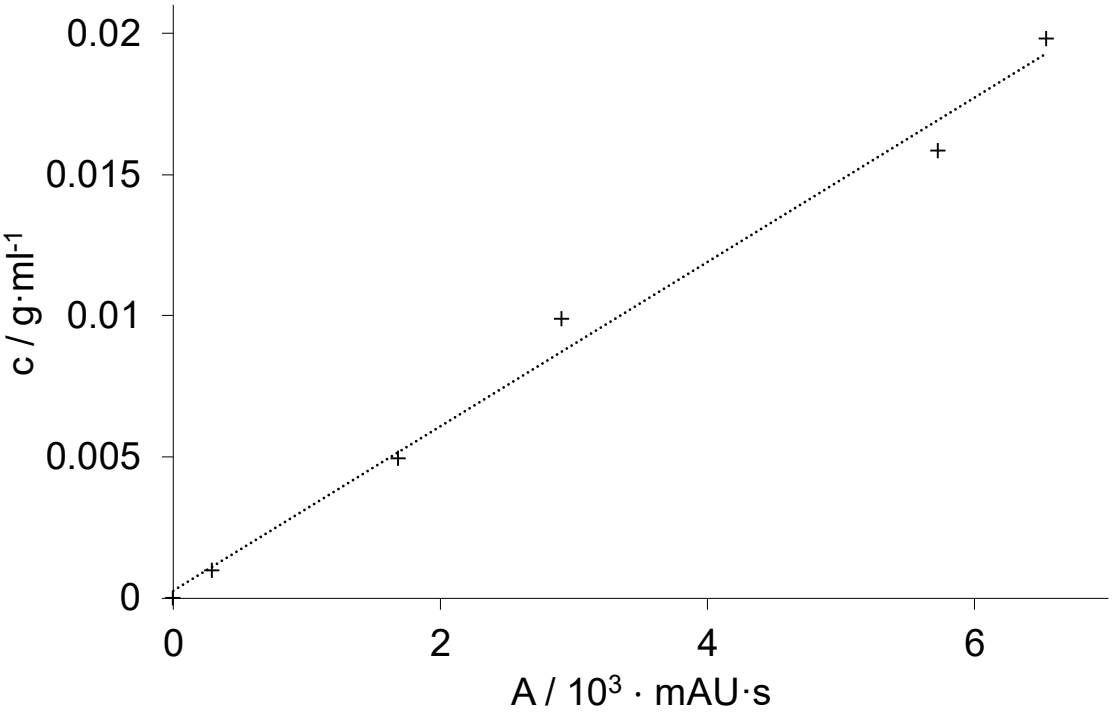

Figure 34. *DAD detector calibration points for 16-hexadecanolide and their linear regression. Slope: $5.862 \cdot 10^{-7}$; intercept: $-7.864 \cdot 10^{-4}$.*

5.4 Synthesis of Tricyclohexylidene triperoxide

A 500 ml three-necked round bottom flask is submerged in a water bath heated by a hotplate stirrer. A Liebig condenser, an addition funnel and a digital thermometer are inserted in each of the flask necks.

4.9 g (0.017 mol) of phosphotungstic acid (PA) are dissolved in 98 g (1 mol, 103.4 ml) of cyclohexanone ($g_{PA.}/g_{CHX} = 0.05$) and put inside the flask. The solution is heated up to 65°C, keeping the system mixed using a magnetic stirrer.

126.8 g (1.1 mol, 114.2 ml) of 30% hydrogen peroxide are weighted ($mol_{CHX}/mol_{H_2O_2} = 0.9$) and introduced inside the funnel. The peroxide is dosed during 15 min drop by drop, in order to maintain the temperature below 70°C. The solution acquires a white colour. The system is left reacting for 5 hours at 65°C.

1 g (0.01 mol) of sodium bicarbonate ($g_{NaHCO_3}/g_{PA.} = 0.2$) is added at the end of the reaction maintaining agitation.

After water cooling, the crude reaction mixture is poured into a separatory funnel.

100 ml (133 g) of dichloromethane[1] are added and the mixture is left separating the phases until two liquid phases appear: an upper aqueous one and a lower organic one. The latter is removed,

[1] Dichloromethane can be replaced with cyclohexane; the result is the same but the separation by density is slower with the latter.

poured in another funnel, extracted by water, decanted and separated again. The aqueous phase is extracted using dichloromethane, decanted and separated. The two organic phases are joined and rotaevaporated. A viscous gel-shape liquid s obtained. It is cooled down and crystallized with methanol.
Crystallization is carried out in a flat bottom flask submerged in a water bath and heated by a hotplate stirrer. The flask is equipped with a double cooling condenser.
100 ml (79.2 g) of methanol are added. The suspension is heated and stirred until it becomes transparent. It is cooled down at ambient temperature and then is left in the fridge at 4°C for at least 12 hours.
The solid is recovered by filtration and dried under vacuum with phosphorous pentoxide.
The final product is analysed by DSC and HPLC as described in §5.3.1 and in §5.3.2.

5.5 Batch experiments

Batch experiments are carried out following the experimental design shown in Table 16**.**

Table 16 *Experimental design of batch experiments based on $L_8(2^5x3^1)$ Taguchi matrix.*

Exp.	Real factors		
	***t* / min**	**w_{TCHTP} / %**	***T* / °C**
1	30	4	150
2	30	4	190
3	30	8	190
4	30	8	150
5	60	4	170
6	60	4	170
7	60	8	170
8	60	8	170

Eight 5 ml vials are filled with the appropriate solution of TCHP in *n*-dodecane. Each vial is closed, put inside a furnace and let inside it at the temperature and for the time indicated in Table 16.
Once a single experiment is finished, the crude reaction mixture is suddenly cooled down in water.
A sample of each vial is collected and analysed via HPLC, according to the procedure described in §5.3.2. When the concentration of triperoxide is greater than 0.04 $g \cdot ml^{-1}$, it is needed to dilute the sample to avoid saturation of the HPLC detector.

5.6 Experiments with tubular reactor

3 m of PTFE tube with internal diameter equal to 0.03" are measured, coiled and immersed into a silicon bath placed inside an oven. The part of the tube in contact with silicon (2 m) and the distance between the inlet-outlet hole and the silicon's edge (0.44 m) totally measure 2.44 m and it is considered to be the active tube length, *i.e.* the one in which the reaction occurs.
The inlet and the outlet are connected to a pump (P-1) and to a sample collection system respectively.
Temperature is measured by a thermometer (TI) put directly inside the silicon bath.
Many series of experiments are carried out. Solutions of 4% w/w of TCHP in *n*-dodecane are prepared on demand from the previously synthetized TCHP and pumped inside the tube using a previously calibrated piston pump and a syringe pump, at different flowrates.
Every time a new reactant mixture is prepared, it is sampled and analysed via HPLC.
For each flowrate the mean residence time is calculated dividing the total volume of the reactor by the volumetric flowrate.
The collection of the sample starts after a heuristically-determined time required to reach the steady state, equal to three times the actual mean residence time.
Table 17 shows all the volumetric flowrates investigated, together with the mean residence time (τ) and the time required to reach the steady state (t_{SS}).

Table 17. *Flowrates (Q / ml·min^{-1}), mean residence time (τ / s) and time required to get the steady state (t_{SS} / min) applied during tubular reactor experiments.*

Q / ml min^{-1}	τ / s	t_{SS} / min
8.00	8	0.4
6.40	10	0.5
4.80	14	0.7
3.20	21	1.0
1.00	67	3.3
0.50	134	6.7
0.30	223	11.1
0.25	267	13.4
0.20	334	16.7
0.18	371	18.5
0.15	445	22.3
0.12	556	27.8
0.10	668	33.4
0.08	835	41.7
0.06	1113	55.6
0.04	1669	83.5
0.05	1335	66.8

Collection time is about one residence time. Each sample is analysed via HPLC according to the method described in §5.3.2.

5.7 Experiments with tube-in-tube reactor

1.85 m of Teflon® AF2400 tube (internal diameter of 0.032") are connected in one of the two same-direction branches of a T- piece (1/8", 1/8", 1/8"). 1.80 m of PTFE tube (internal diameter of 1/8") are inserted into the opposite branch, generating the tube-in-tube layout (Figure 35).

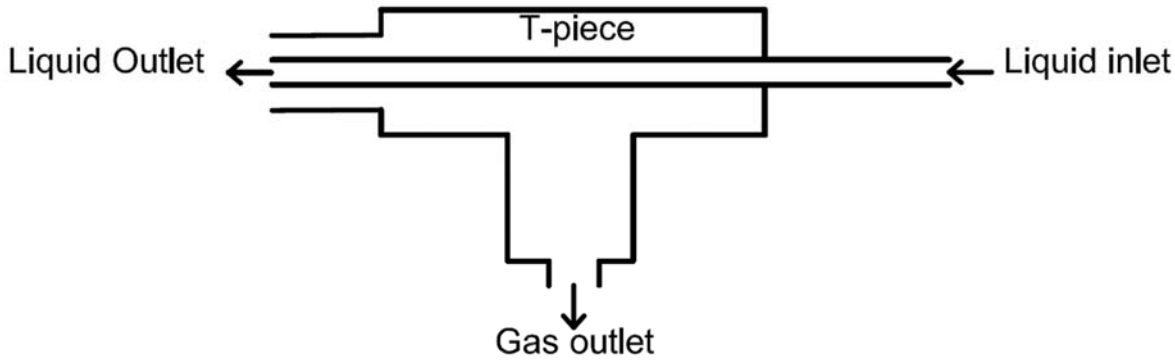

Figure 35. *Schematic representation of one of two T-pieces included in tube-in-tube reactor layout.*

Another "T" piece (1/8", 1/8", 1/8") is installed on the other side of the concentric structure and the tubes are arranged in the same way described above.
One outlet of one "T" piece is connected to a flask and then to a vacuum pump using another 1/8" internal diameter of PTFE tube.
The remaining outlet of the "T" piece is hermetically closed.
Vacuum pump (C-1) allows to put under vacuum the clearance between the two tubes and appropriate ferrules ensure the seal of the system.
The whole system is then placed inside an oven and each extremity of the tube-in-tube reactor is joined to a PTFE tube (ID = 1/16"), providing the inlet (0.75 m inside the oven) and the outlet (0.15 m inside the oven).
High temperature requires customized PEEK ferrules, instead of the standard Teflon® ones used in the previous tubular system.
The inlet tube is connected to a syringe pump (P-1) and 0.35 m (R-2) of it are submerged in a silicon bath. The whole length of the tube-in-tube reactor (R-1) is put inside the silicon bath. The outlet ends in a sample collection system. Temperature is measured inside the silicon bath with a thermometer (TI). A schematic representation of the system is reported in Figure 28 to make the explanation clearer.

Solutions of 4 % w/w of TCHP in n-dodecane are prepared on demand from the previously synthetized TCHP and pumped inside the tube at different flowrates, while the vacuum pump is working. Every time a new reactant mixture is prepared, it is sampled and analysed via HPLC. For each flowrate the mean residence time is calculated. Table 18 shows all the volumetric flowrates used, together with the mean residence time (τ), the time required to reach the steady state (t_{SS}). All those variables have the same meaning of the ones of §5.5.

Table 18. *Flowrates (Q / ml·min^{-1}), mean residence time (τ / s) and time required to get the steady state (t_{SS} / min) applied during tubular reactor experiments.*

Q / ml min^{-1}	τ / s	t_{SS} / min
0.265	295	14.7
0.199	393	19.7
0.159	491	24.6
0.132	590	29.5
0.114	688	34.4
0.099	786	39.3
0.088	885	44.2
0.079	983	49.1
0.072	1081	54.1
0.066	1179	59.0
0.061	1278	63.9
0.057	1376	68.8
0.053	1474	73.7
0.050	1572	78.6
0.047	1671	83.5

Collection time is about equal to one residence time. Each sample is analysed via HPLC according to the method described in §5.3.2.

Conclusions

An experimental design regarding the behaviour of conversion, selectivity and yield as a function of reaction time (A), reagent's initial mass fraction (B) and temperature (C) in batch conditions gives the following information inside the experimental domain:

- Factors A and B have a significant influence on conversion. Temperature is the most important one and it positively affects conversion, even though total conversion was reached both at 170°C and 190°C. Longer reaction time clearly leads to higher conversion.
- Selectivity is affected in a non-negligible way by all factors. Highest values (23 %) were found for T = 150°C, 30 min reaction time and 8 % w/w mass fraction of TCHP.
- Temperature and reaction time are the only relevant factors explaining yield variability. Higher yield is found for higher reaction times and, regarding temperature, for 190°C, but not such a big difference is found for T = 170°C.

For all those reasons, T = 170°C, w_{TCHP} = 4 % w/w and t = 60 min were selected as starting conditions to perform the continuous process of TCHP thermolysis.

Analytical methods to analyse reaction mixture were implemented. DSC was used for thermal characterization of synthetized TCHP. HPLC was used to evaluate the purity of TCHP and to analyse crude reaction mixture. Calibration lines were calculated to obtain TCHP and 16-hexadecanolide concentration. Starting from those experimental data, conversion, selectivity and yield were calculated during reaction progress.

Two flow reactor layouts were designed and built. The first one was a tubular reactor and the second one was a tube-in-tube reactor, thought to extract CO_2 generated during reaction progress.

Two models to predict the conversion profile were implemented in MATLAB®. A plug flow (PFR) model and a laminar flow (LFR) model.

Tubular reactor's conversion profile is not predictable using only one model. Bubble generation affects the system fluid dynamics. At low residence time, PFR model better reproduces experimental data, whereas LFR model is more accurate at higher reaction progress.

Tube-in-tube reactor allows to extract CO_2 and other compounds evaporating at 170°C. The fluid dynamics of the reactor is no more affected. LFR model fits experimental data, providing a reliable way to predict conversion profile in this type of reactor.

The combination of PFR model and LFR model is slightly better in predicting tubular reactor behaviour, but the greater internal coherence of tube-in-tube was demonstrated using a second order polynomial that perfectly reproduce experimental data.

Total yield in 16-hexadecanolide of the two processes is found to be comparable and roughly equal to 18 %.
It is concluded that tube-in-tube reactor allows to perform a safer and reliable process about TCHP thermal decomposition.

Nomenclature

CHX	=	Cyclohexanone
DCHP	=	Dicyclohexylidene diperoxide
DSC	=	Differential scanning calorimetry
FDA	=	Food and Drug Administration
HPLC	=	High performance liquid chromatography
ID	=	Internal diameter
NPK	=	Non-parametric kinetics method
P/TFE	=	Poly/tetrafluoroethylene
PA	=	Phosphotungstic acid
PAT	=	Process analytical technology
PDD	=	2,2-bistrifluoromethyl-4,5-difluoro-1,3-dioxole
PEEK	=	Polyether ether ketone
PT	=	Prout-Tompkins
RO	=	n^{th} order
SB	=	Sěsták-Berggren
TCHP	=	Tricyclohexylidene triperoxide
TI	=	Temperature indicator

Bibliography

Akahira, T. and Sunose, T. (1971) 'Method of determining activation deterioration constant of electrical insulating materials', *Res. Report Chiba Inst. (Sci. Technol.)*, **16**, pp. 22–31.

de Armas, D. (2015) 'Síntesis de macrolactona cíclicas', *PhD Thesis*, IQS School of Engineering (Spain).

Avilés, K. (2004) 'Improvement of an industrial process for the production of cyclic macrolactones (MLC) ', IQS School of Engineering (Spain).

Brzozowski, M. *et al.* (2015) 'Flow Chemistry: Intelligent Processing of Gas-Liquid Transformations Using a Tube-in-Tube Reactor.', *Accounts of chemical research*. American Chemical Society, **48**(2), pp. 349–362.

Bush, P. and Story, P. R. (1970) 'Macrocyclic synthesis.III.Synthesis and reactions of mixed tricycloalkylidene peroxides', *Synthesis*, pp. 181–183.

Cranwell, P. B. O'Brien, M. Browne, D. L. Koos, P. Polyzos, A. Pena-Lopez, M. and Ley S. V. (2012) 'Flow synthesis using gaseous ammonia in a Teflon AF-2400 tube-in-tube reactor: Paal-Knorr pyrrole formation and gas concentration measurement by inline flow titration', *Organic & Biomolecular Chemistry*. Royal Society of Chemistry, **10**, pp 5774–5779.

Dien, J. M. *et al.* (1994) 'The Thermal Risk of Autocatalytic Decompositions: a Kinetic Study', *Chimia*, **48**, pp. 542–550.

Ferrer, N. Serra, E., Sempere, J. and Nomen, R. (2017) 'Non-parametric kinetic analysis of autocatalytic reactions', *Journal of Loss Prevention in the Process Industries*, **49**, pp. 357–366.

Ferrer, N. Serra, E., Sempere, J. and Nomen, R. (2018) 'Thermal decomposition of tricyclohexylidene triperoxide', [Pending review].

Flynn, J. H. and Wall, L. A. (1966) 'A quick, direct method for the determination of activation energy from thermogravimetric data', *Journal of Polymer Science Part C: Polymer Letters*, **4**(5), pp. 323–328.

Food and Drug Administration (2004), "Guidance for Industry PAT - A framework for innovative pharmaceutical development, manufacturing and quality asurance"

Freeman, E. and Carroll, B. (1958) 'The application of thermoanalytical techniques to reaction kinetics. The thermogravimetric evaluation of the kinetics of the decomposition of calcium oxalate monohydrate', *The Journal of Physical Chemistry*, **62**(4), pp. 394–397.

Friedman, H. L. (1964) ‘Kinetics of thermal degradation of char-forming plastics from thermogravimetry. Application to a phenolic plastic’, *Journal of Polymer Science Part C: Polymer Symposia*, **6**(1), pp. 183–195.

Geyer, K., Gustaffson, T. and Seeberger, P. H. (2008) ‘Developing continuous-flow microreactors as tools for synthetic chemists’, *Synlett*, No. 15, pp. 2382–2391.

Kaiser, M. and Ticmanis, U. (1995) ‘Thermal stability of diazodinitrophenol’, *Thermochimica Acta*, **250**(1), pp. 137–149.

Kissinger, H. E. (1957) ‘Reaction Kinetics in Differential Thermal Analysis’, *Analytical Chemistry*. American Chemical Society, **29**(11), pp. 1702–1706.

Mason, B. P. Price, K. E. Steinbacher, J. L. Bogdan, A. R. and McQuade D. T. (2007) ‘Greener approaches to organic synthesis using microreactors technology’, *Chemical. Reviews*. American Chemical Society, **107**, pp 2300–2318.

Nomen, R. *et al.* (2003) ‘Production of macrocyclic lactones through catalytic oxidation of cyclohexanone’, *Journal of Thermal Analysis and Calorimetry*, **72**, pp. 991–1003.

Ozawa, T. (1965) ‘A New Method of Analyzing Thermogravimetric Data’, *Bulletin of Chemical Society of Japan*, **38**(11), pp. 1881–1886.

Paul, K. *et al.* (1976) ‘A new method for the synthesis of biscyclododecylidene cycloalkylidene triperoxides’, *The Journal of organic chemistry*, **41**, No. 7, pp. 1283–1285.

Resnick, P. R. and Buck, W. H. (1997) ‘Modern Fluoropolymers’, in Scheirs, J. (ed.) *Modern Fluoropolymers*. Wiley, pp. 397–419.

Sanderson, J. R. and Story, P. R. (1974) ‘Macrocyclic synthesis.The thermal decomposition of dicyclohexylidene diperoxide and tricyclohexylidene triperoxide’, *The Journal of organic chemistry*, **39**, 24, pp. 3463–3469.

Sanderson, J. R., Story, P. R. and Kalidas, P. (1975) ‘Thermal decomposition of some bis(cyclododecylidene)cycloalkylidene triperoxides in chlorobenzene’, *The Journal of organic chemistry*, **40**, No. 6, pp. 691–695.

Schmidt, L. D. (1998). *The Engineering of Chemical Reactions*. Oxford University Press, Inc. New York (U.S.A.).

Sempere, J., Nomen, R. and Serra, R. (1999) ‘Progress in Non-parametric Kinetics’, *Journal of Thermal Analysis and Calorimetry*. Kluwer Academic Publishers, **56**(2), pp. 843–849.

Serra, R., Nomen, R. and Sempere, J. (1998) ‘The Non-Parametric Kinetics A New Method for the Kinetic Study of Thermoanalytical Data’, *Journal of Thermal Analysis and Calorimetry*. Kluwer Academic Publishers, **52**(3), pp. 933–943.

Serra, R., Sempere, J. and Nomen, R. (1998) ‘A new methods for the kinetic study of thermoanalytical data: The non-parametric kinetics method’, *Thermochimica Acta*, **316**, pp. 37-45.

Story, P. R. *et al.* (1968) ‘A new general synthesis of macrocyclic compounds’, *Journal of the American Chemical Society*, **90**, pp. 817–818.

Story, P. R. *et al.* (1970) ‘Macrocyclic synthesis.II.Cycloheanone peroxides’, *The Journal of organic chemistry*, **35**,No.9, pp. 3059–3062.

Villa, R. (1999) *Ossidazione catalitica del cicloesanone con H_2O_2 (35%)*. Politecnico di Milano.

Vyazovkin, S. and Dollimore, D. (1996) ‘Linear and Nonlinear Procedures in Isoconversional Computations of the Activation Energy of Nonisothermal Reactions in Solids’, *Journal of Chemical Information and Modeling*. American Chemical Society, **36**(1), pp. 42–45.

Williams, A. S. (1999) ‘The Synthesis of Macrocyclic Musks’, *Synthesis*, **1999**(10), pp. 1707-1723.